HEAT TRANSFER STUDY OF POLYMER SOLUTIONS WITH DIFFERENT RIGIDITIES

Thesis

by

YAO HUANG

Submitted to the Office of Graduate and Professional Studies of
Texas A&M University
in partial fulfillment of the requirements for the degree of

Master of Science

Chair of Committee,	Jorge L. Alvarado
Committee Members,	Michael Pate
	Charles Culp
Head of Department,	Andreas A. Polycarpou

May 2014

Major Subject: Mechanical Engineering

ABSTRACT

The heat transfer behaviors of non-Newtonian fluids under laminar flow conditions in circular tubes are presented in this study. The constant wall heat flux is considered as a boundary condition for dilute polymer solutions with different polymer rigidities. A mathematic method was introduced to model the rigidity of polymer chain's effect on the dynamic viscosity of dilute polymer solution. Results were also obtained for the dilute polymer solutions under both hydro-dynamically developing and hydro-dynamically developed conditions. In case of a smooth circular tube with dilute polymer solution, the results of Nusselt numbers and fanning friction factors were obtained by varying initial Reynolds number and polymer rigidity. The effects of the polymer rigidity and the Reynolds number on the Nusselt number were found to be small. It was also observed that the friction factor and the performance evaluation criteria were strongly dependent on both polymer rigidity and Reynolds number.

DEDICATION

To my family for their love, support and understanding

ACKNOWLEDGEMENTS

I would like to express my sincere gratitude to several people who made this thesis possible. First of all, I would like to thank my advisor, Dr. Jorge Alvarado, for sparing his time and sharing his knowledge on the subject with me. I would like to thank my committee member, Dr. Michael pate and Dr. Charles Culp, for their valuable input.

I also want to thank Qibo Li for his kind support in sharing his knowledge and help with solving software problems in GAMBIT.

In addition, I want to thank my parents, Mr. Qingsong Huang and Mrs. Xianyu Zou, my friends, and my other family members for encouraging me to persist for higher education. My parents, friends, and family members have been the supporter in difficult times and always believed in my capabilities.

NOMENCLATURE

Variables

C	Mass concentration
C_p	Specific heat
D	Diameter of the tube
f	Fanning friction factor
g	Acceleration of gravity
Gz	Graetz number
Gr	Grashof number
n	Flow index
K	Consistency index
k	Thermal conductivity
L	Tube length
L_k	Kuhn length
$\dot{m}$	Mass flow rate of the slurry or fluid
m	Rigidity changing parameter

Nu	Nusselt number
L_c	Contour
Pr	Prandtl Number
q	Heat
q"	Heat flux
<R>	End-to-end vector
r	Radius of the tube
T	Temperature
T_b	Bulk temperature
T_w	Temperature at a distance z from the inlet
u	Velocity in x direction
v	Velocity in y direction
w	Velocity in z direction
x	Cartesian co-ordinate along x direction
y	Cartesian co-ordinate along y direction
z	Cartesian co-ordinate along z direction

Greek symbols

$\dot{\gamma}$	Shear rate
ϕ	Volumetric concentration
θ	Rotation angle
η	Dynamic viscosity
ρ	Density

Subscripts

b	Bulk
eff	Effective
H	Constant wall heat flux
i	Inlet
mean	Mean
w	Wall

Acronyms

CC	Chemical Composition
CS	Chemical Structure
DPS	Dilute Polymer Solution
MW	Molecular Weight
RCP	Rigidity Changing Parameter

TABLE OF CONTENTS

Page

LIST OF FIGURES

Page

LIST OF TABLES

Page

INTRODUCTION

1.1 Non-Newtonian Fluids

A number of fluids such as rubber, plastics, synthetic fibers, petroleum, and paints are non-Newtonian fluids because their viscosity properties are fluid shear rate dependent [1]. The study of convective heat transfer of non-Newtonian fluids has been attracting considerable interests among many investigators due to its relevance in industrial applications, including their use in industrial heat exchangers, certain HVAC systems, chemical industries, petroleum industries and food industries, to name a few. As a result a great number of investigations have studied the rheological behavior and heat transfer of non-Newtonian flow in circular pipes under different boundary conditions.

It is known that for Newtonian fluids, the shear stress τ is linearly dependent on shear rate $\dot{\gamma}$ [1] ， as given by:

$$\tau = -\mu \dot{\gamma} \tag{1}$$

Here τ is the shear stress, μ is the fluid's dynamic viscosity.

For non-Newtonian fluids, the viscosity μ varies with shear rate, so the rheological behavior is certainly more complicated. Due to the relationship between shear stress and shear rate, non-Newtonian fluids can be split into three categories [2],

(a) time-dependent non-Newtonian fluid

(b) time-independent non-Newtonian fluid

(c) viscoelastic non-Newtonian fluid

Time-independent non-Newtonian fluids, whose shear rate at a given point are only dependent upon the instantaneous shear stress. These kinds of fluids can also be characterized by having an initial yield stress including Bingham plastic fluids [3] and Herschel-Bulkley fluids [4]; and fluids without a yield stress including pseudoplastic fluid, whose viscosity decreases when shear rate increases. On the other hand the viscosity of dilatant fluids increases when the shear rate increases. Classic time-independent fluids are depicted in Fig. 1.1

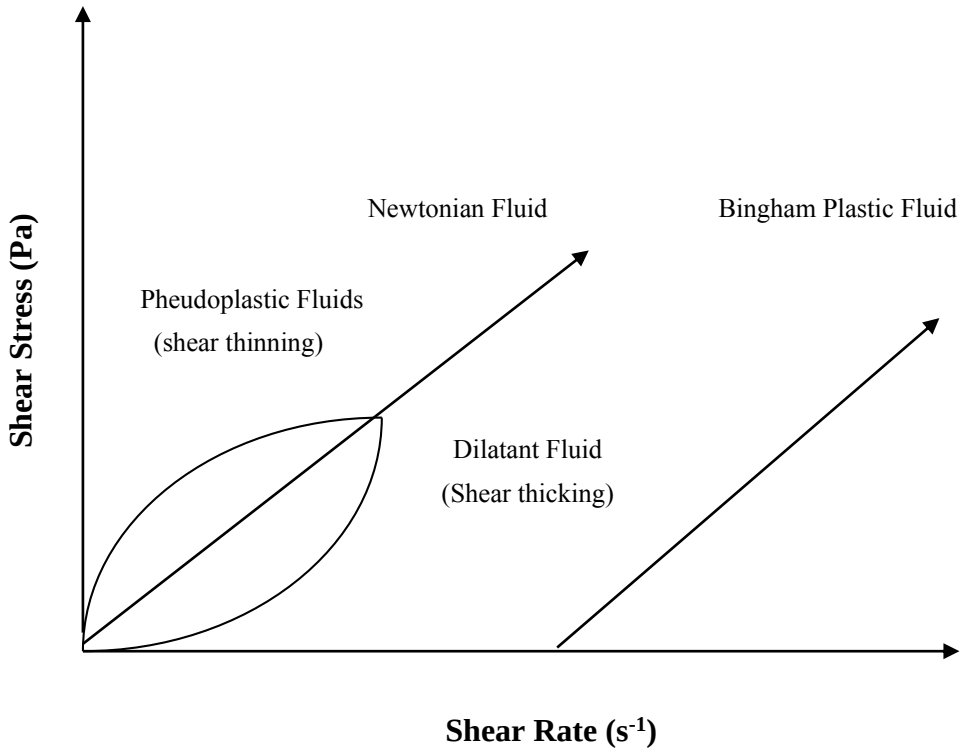

Fig. 1.1 Comparison of time-independent non-Newtonian fluids

Time-dependent non-Newtonian fluids are characterized by having a more complicated relationship between shear rate and shear stress where the shear stress can change with time at a given shear rate. These fluids are usually classified into two types: thixotropic fluids and rheopectic fluids.

Viscoelastic fluids have both viscous and elastic properties. In contrast to purely viscous liquids, they will flow when subjected to stress, but its initial viscosity behavior cannot be fully recovered upon removal of the shear stress. To describe these sort of fluids, we need not only to understand the relationship between shear stress and shear rate, but also the time derivatives of both properties.

In our research, time-independent non-Newtonian fluids have been considered for flow and heat transfer simulations. A number of studies, both experimental and theoretical, have been performed using viscosity models for non-Newtonian fluids. O. Waele [5] first introduced the power law model for time-independent non-Newtonian fluids shown in equation (2):

$$\tau = k\dot{\gamma}^n \tag{2}$$

Where τ is the shear stress, k is the consistency index, n is the flow index. Both k and n are determined by experimental methods.

The power law model describes well the shear thinning behavior of pseudoplastic fluids; however, the Equation fails to capture the viscosity behavior of the fluid when the shear rate becomes relatively large or small. For n greater than one, the viscosity of the

fluid will approach zero near the zero shear rate region, which does not reflect the physical behavior of the fluid.

1.2 Polymer Solution

In this study, dilute polymer solutions have been considered since the effects of polymer rigidity on hydrodynamics and convective heat transfer are still unknown. A polymer is characterized by having large number of monomers, and the molecular weight can be substantial. Classic natural polymeric materials such as natural fiber, rubber, and hides have been commonly used for centuries. During the 19^{th} century, chemists developed synthetic polymer molecules by polymerization reactions.

In general, polymer solution is a liquid mixture of long and large polymer molecules, and light solvents. Polymer solutions are non-Newtonian fluids, characterized by having a complicated rheological properties.

1.3 Motivation for Current Work

The study of rheological behavior of polymer solutions in circular pipe is an important issue due to its wide application in heat transfer, biochemistry, automotive industry and

chemical industry. The microstructure and molecular weight of polymer molecules can affect the viscosity of polymer solutions. Similarly, the rigidity of long molecule chains can also affect the rheological behavior of polymer solutions. Thus a thorough understanding of the relationship between polymers structural properties and the characteristic non-Newtonian flow behavior in circular pipe is of fundamental importance to a host of engineering applications.

After a thorough literature survey in areas of polymer science and non-Newtonian fluids, it was found that both experimental and numerical analyses are still lacking in the study of the relationship between polymer rigidity and rheological behavior of polymer solutions. Therefore, the study of the effect of the rigidity of polymers in dilute polymer solutions on convective heat transfer and pressure drop in a circular pipe was undertaken.

1.4 Aim and Objective

The objective of the current study was to determine the effect of polymer rigidity on viscosity, convective heat transfer and pressure drop. As the first step, two types of classical non-Newtonian fluids were simulated using CFD software to numerically validate the flow behavior of such fluids in a circular pipe with axially and peripherally uniform heat flux along the wall. Then, a comparison between the well-published

convective heat transfer correlations and the ones obtained numerically was made in order to gain better understanding of non-Newtonian fluids.

The second step consisted of understanding thoroughly the effect of polymer structures on viscosity. A detailed mathematical method was used to determine the effect of molecular structure of polymers on polymer rigidity and the viscosity of dilute polymer solutions. The relationship between polymer chain rigidity and viscosity of the fluid was analyzed using existing polymer theories.

The next step consisted of simulating the flow of dilute polymer solutions in a circular pipe under constant heat flux conditions. Polymer solutions with the same concentration and molecular weight but different polymer rigidity were simulated. The effects of polymer rigidity on viscosity, convective heat transfer and pressure drops were evaluated based on the simulated results.

LITERATURE REVIEW

In this section, research background of the non-Newtonian fluid and polymer science are presented. The section has been divided into four parts. The first part brings a brief introduction of classic viscosity models of non-Newtonian fluids. The second part focuses on previous experiments and study of heat transfer of non-Newtonian fluids. The third part discusses the study of polymer structures. In addition, the fourth part focuses on the effect of the polymer rigidity on the dynamic viscosity.

2.1 Viscosity Model of Non-Newtonian Fluid

Numerous studies have been done on the prediction of the viscosity models of non-Newtonian fluids. Waele [5] introduced the power law model which can describe well the viscosity variation in limited shear rate regions. Because of the limitation of the Power-law model, other non-Newtonian models have also been developed to meet the requirements for describing multiple types of fluids.

Carreau et al. [6] proposed a viscoelastic model extrapolated from the generalized Maxwell model. In their work, viscoelastic fluids such as polymer melts and solutions can

be generally described by Maxwell model which they used to develop the Carreau-Bird model. His model is based on several assumptions including the use of zero shear rate viscosity, infinite shear rate viscosity, and relaxation time. Compared with the Power-law model, the Carreau model is more useful when studying fluids with non-Newtonian viscosity in high shear rate and Newtonian viscosity in low shear rate.

Mongruel et al. [7] studied xanthan solution, which is a classic semi-rigid polymer solution (non-Newtonian fluid), with low concentrations flowing through an axisymmetric orifice. In his work, the Carreau model was utilized to provide theoretical analysis of the elongational viscosity of the xanthan solution. Supported by experimental data, the author claimed that the Carreau model is available to predict the elongational viscosity of semi-rigid polymer solution.

The Herschel–Bulkley model was introduced in 1926. The relationship between shear stress and shear rate in the model is characterized by consistency index k, the flow index n, and yield shear stress. The Herschel–Bulkley model can be used to analyze Non-Newtonian fluids specifically with yield stress.

Casson model was developed by Casson in 1959, originally to study flow behavior of pigment-oil suspensions. The Casson model can reveal both shear thinning and yield stress, and it has been frequently used for the study of food products. Pastor et al. [8] used xanthan

gum solutions in their experiments. In their work, 48 samples of xanthan solutions with different pH conditions, concentrations and initial inlet velocities had been analyzed. The Casson model and the power law model were used to provide theoretical analysis in their study. It was found that the pH number and concentration can both affect the viscosity of xanthan solution, and both the Casson model and the power law model can be utilized to describe the polymer solutions' rheological behaviors.

Cross model [2] was proposed by Cross (1965), which is a four constant model, which displays a non-zero bounded viscosity at both the upper and lower shear rate limits. In shear thinning region the Cross model fluid behaves like a Power-law fluid, but it can produce Newtonian viscosity at relatively low or high shear rate regions.

The Ellis model was introduced in limited papers [9] which set the viscosity with extremely large shear rate to zero for simplification. Until now, the most commonly used non-Newtonian model is the Power-law model, given a certain zero shear rate and an infinite shear rate viscosity limitations, The Power-law model can well describe the shear thinning behavior of pseudoplastic non-Newtonian fluids in CFD simulation.

2.2 Heat Transfer of Non-Newtonian Fluids

Flow and heat transfer of fluids with Non-Newtonian properties have evoked proper consideration of investigators in the past and are still a point of discussion in recent years. Metzner et al. [10] conducted experiments to study the relationship between Graetz number [11] and Nusselt number in 1957. In their work, dilatant and pseudo-plastic fluids were tested, and an expression of Nusselt number was presented involving the flow index and the Graetz number.

Both experiments and numerical analysis were undertaken by Mahalingam et al. [12-13] in 1974. Three different materials including water, Methocel, and Carboxypolymethylene were tested in long, circular pipes with constant wall heat flux boundary condition. Comparisons were made between previous theoretical Nusselt number and the experimental data. The author claimed that the experiment data can well meet with the theoretical prediction of Nusselt number. The expression of Nusselt number for that type of non-Newtonian fluid is:

$$Nu = 1.418 \cdot \left(\frac{3n+1}{4n} \right)^{\frac{1}{3}} \cdot (Gz)^{\frac{1}{3}} \tag{3}$$

Where Nu is the Nusselt number, n is the flow index of power law fluid, Gz is the Graetz number, which can be expressed in Equation (4):

$$Gz = \frac{\dot{m}C_p}{kL} \tag{4}$$

Where $\dot{m}$ is mass flow rate, k is thermal conductivity, L is hydraulic diameter，and C_p is heat capacity. It can be observed that the consistency index of Power-law model has no effect on heat transfer coefficient since it does not appear in the Nusselt number equation. It was found that when Graetz number is between 100 and 10000, the Equation (4) can well describe the Nusselt number of power law fluid under constant wall heat flux boundary condition.

Cruz et al. [14] proposed an approximate methodology for different non-Newtonian models to estimate the Nusselt number and friction factors. To get the Reynolds number and the Nusselt number, the wall shear rate, bulk velocity, apparent flow index were used and the error was within 3.2% compared with previous data.

Chhabra [15] gave detailed analysis and experimental data for velocity profile and Nusselt number calculation. In his book, the velocity profile for full developed Power-law fluid in a tube is given by Equation (5):

$$V_z = V\left(\frac{3n+1}{n+1}\right)\left[1-\left(\frac{r}{R}\right)^{(n+1)/n}\right] \tag{5}$$

Where, V_z is the velocity in axial direction, V is the mean velocity of flow, r is radial distance from axis, R is radius of tube, n is flow index of Power-law model. The Nusselt number is given by Equation (6):

$$Nu = 1.75 \cdot \left(\frac{3n+1}{4n} \right)^{1/3} \cdot Gz^{1/3} \tag{6}$$

Equation (6) is used specifically for limited conditions with relatively large Graetz number (larger than 10000).

A number of scientists also studied heat transfer of Non-Newtonian fluids in equipment with specific shapes. Escudier et al. [16] conducted experiments and made comparison between numerical solution and experimental data of the non-Newtonian flow through an annulus pipe. Chung et al. [17] studied numerical solution for the Power-law flow in rectangular ducts with different boundary conditions. Salem et al. [18] presented theoretical and experimental investigation for laminar and turbulent of both Newtonian fluids and non-Newtonian fluids through non-circular pipes. Pascal et al. [19] developed non-linear equations to describe transient flow of Power-law fluids through a porous medium. Suckow et al. [20] gave numerical analysis for heat transfer to polymer solutions and melts that flow between parallel plates. However, no studies have been undertaken to

understand the effect of polymer rigidity of dilute polymer solutions on heat transfer performance of heat transfer fluids.

2.3 Polymer Structure and Rigidity

Polymer structure was first reported by Hermann Staudinger [21] in 1920. It was found that polymer materials, including rubber, proteins, and fibers are formed by long chain molecules with repeating subunits linked by covalent bonds. W. Kuhn, E. Guth, and G. Mark [22] tested the elasticity phenomenon during stretching of polymer sample, and their ideas brought about the prediction that the micro conformational statistical properties of polymer molecules can have influence on the complex physical properties of polymers as a whole.

Kuhn developed random walk model for polymer molecules. In his work, a real polymer chain is considered to be series of segments with an average length *b* (the Kuhn length). Each segment is assumed to be freely joined with each other and the rotation angle for each segment is independent with the position of the other segments. Kuhn length can be determined by end-to-end distance of a polymer chain and the number of segments, it can also represent the rigidity of polymer chain.

To better investigate the polymer chains' contribution to the dynamic properties, Debye [23] simplified the molecule chain to a bend-chain model. In his theory, a polymer chain can be understood as a collection of N rods and N+1 beads. In polymer solution, each unit will have bend resistance, which gives explanation of solution's viscosity. However, the bend chain model does not take into account the effect of hydrodynamic interactions between molecules. The solvent molecules would slow down when they flow through the polymer chains.

Zimm and Rouse [24-25] made an improved model based on Debye's theory. The bead-spring model was carried out to characterize the viscoelasticity of polymer solution. In this theory, a polymer chain is considered to be a collection of flexible Hooke springs and beads. When a polymer chain is moving in a solution, not only the resistance of beads but also the elasticity of polymer chain are taken into consideration. The disadvantage of the bead-spring model is that it cannot explain the phenomenon of shear thinning because of complicated factors such as hydro-interaction effects.

For semi-rigid polymers, Kratky et al. [26] developed the wormlike chain model. In their work, a semi-rigid polymer chain is simplified to be a collection of isotropic rods, in contrast to the freely joint model that only discrete segments are flexible. The wormlike chain model has been adopted as a useful approximate method to study equilibrium and

nonequilibrium behaviors of rigid or semi-rigid macromolecules, such as xanthan gum, and DNA molecules in solutions.

To gain an understanding of rigid polymer chains, such as isotactic polypropylene, and protein in helical forms, the rigid dumbbell model [27] was adopted to give numerical and statistical analyses of polymers. Similar with bend-chain model, the rigid dumbbell makes a simplification that polymer chains are combination of subunits, each subunits consists of two point masses joined by massless rigid rod. The models are the simplification of the true system, but they can be used to predict the behavior of rigid polymer solutions.

To study polymer rigidity, which is one of the most important properties of polymer chain, Guiver et al. [28] investigated the effect of polymer chain rigidity on microporous membranes. Torres et al. [29] conducted both experiments and numerical analysis to study the effect of chain stiffness on the thermal properties and mechanical properties of polymer thin films. The elastic modulus and glass transition temperature were investigated by using 2-phenylethylnorbornene. It was found that by changing the relative flexibility of the side chains would not improve the thin film behaviors. However the main chain rigidity plays an important role in observed changes in physical properties. Another experiment set by Harrison et al. [30] also showed the connection between polymer rigidity and spray

atomization, indicating that the polymer rigidity can have influence on multiple physical properties of the materials.

Jan et al. [31] presented results of molecular dynamic simulations of polyelectrolyte solutions. In their work, the bead-spring model was utilized to study the chain persistence length. The simulations indicate that the polymer chain size is dependent on polymer concentration, salt concentration of the solvent, and solution ionic concentration.

A comprehensive numerical study on modeling of polymer rigidity was done by statistical analysis based on Kuhn's model. The length of each segment has influence on the end-to-end distance of a polymer coil in polymer solution. The dependency of radius of gyration on the average end-to-end distance was discussed by Teraoka [32]. In addition, Kok et al. [33] illustrated the relationship between the radius of gyration of a polymer and hydrodynamic radius in polymer solution.

Gennes [34] investigated the relationship between polymer coils and polymer concentrations. It was found that when the polymer concentration is relatively low, polymer coils will be separated from each other because of the interaction with solvent molecules. In contrast, in concentrated polymer solution, there are entanglements between coils and polymer chains. Predictions of for the coil overlapping concentration were also made to determine the conformation of polymer coils in the solution.

2.4 Intrinsic Viscosity

The intrinsic viscosity is a dimensionless parameter to measure the contribution of a solute to the viscosity of a solution. The intrinsic viscosity can be defined by Equation (7):

$$[\eta] = \lim_{\phi \to 0} \frac{\eta - \eta_0}{\eta_0 \phi} \tag{7}$$

Where $[\eta]$ is the intrinsic viscosity, η is the viscosity of the solution, η_0 is the viscosity in the absence of the solute.

Higiro et al. [35] describes how the multiple main extrapolation methods can be used to calculate the intrinsic viscosity from dynamic viscosity. In their work a comparison was made among the five methods and the authors recommend a method that was developed by Mcmillan in 1974 using the following Equation:

$$\frac{\eta}{\eta_0} = 1 + [\eta] \cdot \phi \tag{8}$$

The author claimed that the Equation 8 showed a better linear fit, with higher correlation for most of the blends, salts and polymer solutions.

Einstein [36] proved the fact that the size and the shape of the particles are the main factors that can affect the viscosity of polymer solutions. The size of the coil is decided by

the radius of gyration, which is dependent on multiple properties of polymer molecules. *Chong* et al [37] introduced the relationship between the radius of gyration and the hydrodynamic radius, through their idea, the radius of gyration and the hydrodynamic radius are linearly dependent for given concentrations. The relationship between the end-to-end distance of polymer chain and the hydrodynamic radius was introduced by Teraoka as indicated above.

The background study suggests that virtually no study has been done on the effect of polymer rigidity on the viscosity of Non-Newtonian fluids. The current study considered dilute polymer solutions consisting of flexible and rigid polymers as heat transfer fluids. Numerical simulations have been undertaken using a smooth circular pipe under uniform heat flux conditions.

DESCRIPTION OF DILUTE POLYMER SOLUTION (DPS) FORMULATION AND NUMERICAL HEAT TRANSFER AND FLUID DYNAMICS SIMULATION SCHEME FOR DPS

3.1 Formulation of the Convective Heat Transfer Problem

In this section the governing equations and the assumptions utilized in modeling the non-Newtonian flow in uniformly heated circular pipe is discussed.

3.1.1 Governing Equation

The modeling of a non-Newtonian fluid in circular pipe with constant heat flux along the wall is based on discretization of the continuity, momentum and energy equations given as follows:

$$\nabla \cdot v = 0 \tag{9}$$

$$\rho v \cdot \nabla v = -\nabla p + \nabla \cdot \tau \tag{10}$$

$$\rho c_p v \cdot \nabla T = k \nabla^2 T + \tau \cdot \nabla \tau \tag{11}$$

Here v is the velocity vector, ρ is the scalar pressure, t is the τ stress tensor, r isthe density of fluid, C_p is the fluid's specific heat, k is the thermal conductivity, and T is the temperature.

The above equations are solved using the finite volume method. The equations were solved numerically by using FLUENT 14.0, which is a commercial and academic computational software used for solving practical fluid dynamics and heat transfer problems. A description of the numerical scheme can be found below.

3.1.2 Assumptions

Various assumptions were made to solve the heat transfer problem for dilute polymer solutions taking into account different polymer chain rigidities.

The non-Newtonian fluids (xanthan-water solution) used in the simulation were assumed to be temperature-independent. This assumption was found to be valid because the average temperature difference between the inlet and the outlet of the simulated system (pipe) was limited to 10 °C, thus the effect of temperature on the physical properties of the non-Newtonian fluid was assumed to be negligible.

The polymer chains that made up the dilute polymer solutions (DPS) were assumed to show no signs of entanglement as long as the concentration in the DPS was less than

0.5%. This assumption simplifies the modeling of polymer rigidity of polymer macromolecules, which are assumed to form independent coils in the solution by ignoring the entanglement between polymer chains. This assumption allows the use of coil size as the main factor that affect the viscosity of DPS.

Polymer coils are assumed to be ideal spheres in DPS with a prescribed radius of gyration, which can be measured experimentally. The rigidity of polymer chains in DPS is assumed to be an adjustable parameter that is completely independent from other physical properties.

Other assumptions include constant thermal conductivity and density. These assumptions allowed treating non-Newtonian fluids as homogeneous liquids.

3.2 Development of Viscosity Model for DPS

3.2.1 Rigidity of Polymer Molecule

The rigidity of polymer chains is governed by the ability of the sub-units in the polymer molecules to rotate around the bonds. Flexible polymer molecules have large rotation angles, in contrast to rigid polymer molecules which have smaller rotation angles. To describe the rigidity of polymer chains, we can directly use rotation angle, but in practice scientists usually use other properties, such as the persistence length.

The persistence length is a basic mechanical property qualifying the stiffness of polymer chain, which is defined in Equation (12),

$$\langle \cos\theta \rangle = e^{-(L/P)} \tag{12}$$

Where θ is the angle between a vector that is tangential to the polymer at position 0 (zero) and a tangent vector at a distance L away from position 0, along the contour of the chain. P is the persistence length and L is the distance between two tangent vectors. The angle corresponds to the average angle when all the vectors can be presented by a single persistence length.

In polymer science, the persistence length can be directly used to determine the polymer rigidity, and it is usually considered to be replaced by the Kuhn lengthsincethe Kuhn length can be obtained experimentally. Equation (13) relates Kuhn length to contour length of the polymer chair as follows:

$$l_k = \langle R^2 \rangle / L_c \tag{13}$$

Here l_k is the Kuhn length. R is the end-to-end vector of N-segment freely jointed chain (each segment of ls). L_c is the contour length of the chain.

The Kuhn length model, or random walk model, was developed by Kuhn [23] to account for the morphology of polymer chains. In his theory, a real polymer chain is defined as a collection of *N* segments, and every one of these segments is freely jointed with each other and independent of the directions taken by the other segments. Instead of considering a real chain consisting of *n* bonds and with fixed bond angles, torsion angles, or bond lengths, Kuhn considered a Hyan equivalent ideal chain with *N* connected segments, now called Kuhn segments that can orient in any random direction.

The random walk model can be seen in Fig. 3.1 as follows:

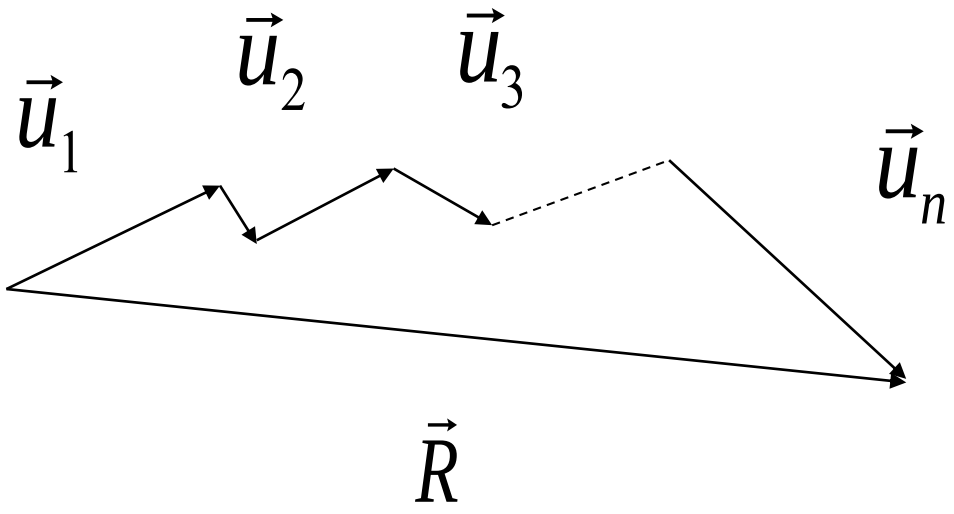

Fig. 3.1 Random walk model

Here R is the end-to-end vector, u_i (i=1, 2, 3....N) is segment with length b. Each nod represents a subunit of the polymer chain. Then the average end to end distance $<R^2>$ is given in equation (14):

$$R^2 = \left(\sum_{i=1}^{N} \vec{u}_i\right) \cdot \left(\sum_{i=1}^{N} \vec{u}_j\right) = \sum_{i=1}^{N}\sum_{j=1}^{N} \vec{u}_i \vec{u}_j \tag{14}$$

$$\left\langle R^2 \right\rangle = \sum_{i=1}^{N}\sum_{j=1}^{N} \left\langle \vec{u}_i \vec{u}_j \right\rangle = \sum_{i=1}^{N} \left\langle \vec{u}_i^2 \right\rangle + \sum_{i=1}^{N}\sum_{j=1}^{N} \left\langle \vec{u}_i^2 \vec{u}_j^2 \right\rangle \tag{15}$$

To expand this equation, the angle between each segment was taken into account to determine R^2. The rotation angle θ is shown in Fig. 3.2.

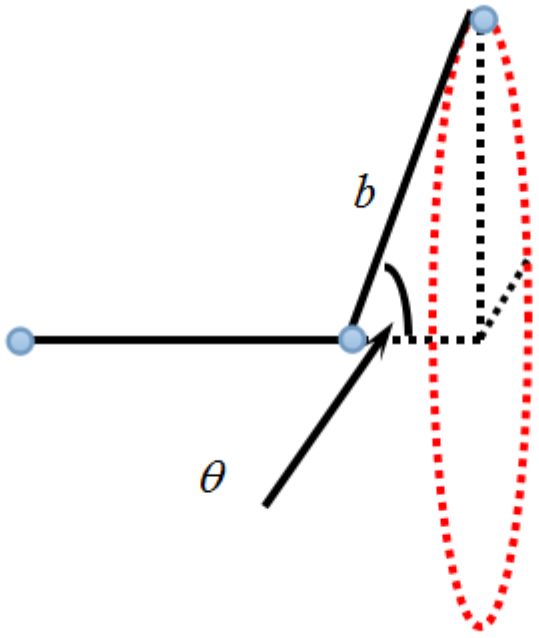

Fig. 3.2 Rotation angle between two segments

In this model (Fig.3.2), the relationship between the vectors and the rotation angles are given in Equations (16-17)

$$\left\langle \vec{u}_i \vec{u}_j \right\rangle = b^2 \left\langle \cos\theta_{ij} \right\rangle \tag{16}$$

$$\left\langle \cos\theta_{i,i+1} \right\rangle = \cos\theta \tag{17}$$

Here θ_{ij} is the angle between segments i and j. By mathematical transformation the angle between segment i and segment $(i+k)$ is given now in Equation (18)

$$\left\langle \cos\theta_{i,i+k} \right\rangle = \left(\cos\theta\right)^k \tag{18}$$

Then the $\langle R^2 \rangle$ can be found as follows:

$$\begin{aligned}
\left\langle R^2 \right\rangle &= Nb^2 + 2b^2 \sum_{i=1}^{N} \sum_{k=1}^{N-i} \left\langle \cos\theta_{i,i+k} \right\rangle \\
&= Nb^2 + 2b^2 \sum_{i=1}^{N} \sum_{k=1}^{N-i} (\cos\theta)^k \\
&= Nb^2 + 2b^2 \sum_{i=1}^{N} \frac{\cos\theta}{1-\cos\theta} \\
&= Nb^2 + 2Nb^2 \frac{\cos\theta}{1-\cos\theta} \\
&= Nb^2 \frac{1+\cos\theta}{1-\cos\theta}
\end{aligned} \tag{19}$$

Equation (19) was also introduced by Alexander and Alexei [22], also by definition the contour length L_c is given in Equation (20),

$$L_c = Nb \tag{20}$$

Applying Equation (19-20), then the kuhn length can be determined as follows:

$$L_k = b\frac{1+\cos\theta}{1-\cos\theta} \tag{21}$$

In this equation, θ is the rotation angle or valence angle. In this model, the persistence length P is shown in Equation (21).

$$p = \frac{b}{\left|\ln(\cos\theta)\right|} \tag{22}$$

By comparing equation (21) and (22), it can be concluded that once the rotation angle is determined, the Kuhn length and persistence length are linearly dependent.

Thus the Kuhn length can be used to describe the rigidity of polymer chain.

3.2.2 Coil Size

The coil size is decided by the average end-to-end distance $<R^2>$. The volume of the coil V is described in Equation (23):

$$V = \frac{4}{3}\pi R_h^3 \tag{23}$$

Here R_h is the hydrodynamic radius of polymer chain. It was proved by Kok and Alfred [35] that the hydrodynamic radius is linear dependent on the radius of gyration (R_g).

$$R_h = c_1 R_g \tag{24}$$

Where c_1 is a constant. The mean radius of gyration ($<R_g^2>$) of a polymer coil is defined as the average square distance of the chain segments from the center of the mass of the chain. It characterizes the size and shape of the polymer and thus it may be obtained from hydrodynamic measurements.

Alexander and Alexei [22] claims that there is a linear dependence between the end-to-end distance and the radius of gyration, when the number of subunit in polymer chain is large enough. The definition of the radius of gyration is given in Equation (25).

$$R_g^2 = \frac{1}{N}\sum_{i=1}^{N}(\vec{r}_i - \vec{r}_g)^2 \tag{25}$$

Where $\vec{r}_i$ is the vector of the *i* th subunit, $\vec{r}_g$ is the center of mass of the coil which is given in Equation (26)

$$\vec{r}_g = \frac{1}{N}\sum_{i=1}^{N}\vec{r}_i \tag{26}$$

By applying Equation (25-26), Alexander and Alexei gave the relationship between R_g and R for ideal coil in Equation (27).

$$\left\langle R_g^2 \right\rangle = \frac{1}{6}\left\langle R^2 \right\rangle \tag{27}$$

Then by applying Equation (23) (27), the connection between the end-to-end distance and the Kuhn length of the polymer chain is given in Equation (28).

$$\begin{aligned} R_h &= c_1 R_g \\ &= c_2\sqrt{\left\langle R^2 \right\rangle} \\ &= c_3\sqrt{\left(L_c L_k\right)} \end{aligned} \tag{28}$$

Where c_1, c_2 and c_3 are constants.

Combining Equation (23) and Equation (28), the relationship between the Kuhn length and the volume of the polymer coil can be obtained as shown in Equation (29).

$$V_h = \frac{4}{3}\pi R_g^3$$
$$= c_4 R^3 \qquad (29)$$
$$= c_5 \left(L_k\right)^{3/2}$$

Where c_4 and c_5 are constants.

3.2.3 Intrinsic Viscosity

The intrinsic viscosity is the solute's contribution to the viscosity of the whole solution as defined in Equation (30). It can be determined experimentally from measurements of the viscosity of very-low-concentration solutions [8].

$$\eta_{\text{intrinsic}} = \lim_{\phi \to 0} \frac{\eta_{\text{solution}} - \eta_{\text{solvent}}}{\eta_{\text{solvent}} C} \qquad (30)$$

Where C is the mass/volume concentration. Einstein [36] introduced Equation (31) which shows the influence of concentration on the viscosity of the fluid.

$$\eta_{solution} = \eta_{solvent}\left(1 + 2.5\phi + 14.1\phi^2 + \cdots + c\phi^n\right) \qquad (31)$$

Where $\eta_{solution}$ is the dynamic viscosity of polymer solution, $\eta_{solvent}$ is the solvent's viscosity, and ϕ *i*s the volume fraction of particles in the system.

For dilute polymer solution, the higher power of concentration in the equation can be neglected, and the Equation (31) is simplified as Equation (32):

$$\eta_{solution} = \eta_{solvent}(1 + 2.5\phi) \tag{32}$$

Where the volume fraction can be represented by Equation (33) assuming each coil to consist of N particles (monomer units) of mass m with a density of ρ.

$$\begin{aligned} \phi &= \frac{N_A C}{mN} V_h \\ &= \frac{C N_A}{M} V_h \end{aligned} \tag{33}$$

where M is the molecular mass of the polymer chain, m is the mass of each polymer subunit, N is the number of subunit, N_A is Avogadro number (6.02214×10^{23}), and V_h is the hydrodynamic volume of the coil.

Applying Equations (29-33) into Equation (30), the relationship between intrinsic viscosity and the hydrodynamic volume of coil is given in Equation (34).

$$\begin{aligned}
\eta_{intrinsic} &= \lim_{\phi \to 0} \frac{\eta_{solution} - \eta_{solvent}}{\eta_{solvent} C} \\
&= \lim_{\phi \to 0} \frac{\eta_{solvent}(1 + 2.5\phi) - \eta_{solvent}}{\eta_{solvent} C} \\
&= \lim_{\phi \to 0} \frac{2.5\phi}{C} \\
&= 2.5 \cdot \frac{CN_A}{M} V_h \cdot \frac{1}{C} \\
\eta_{instrinsic} &= 2.5 \cdot \frac{N_A}{M} V_h
\end{aligned} \tag{34}$$

By combining Equation (29) and Equation (34), the intrinsic viscosity's dependence on the Kuhn length is given by Equation (35)

$$\begin{aligned}
\eta_{\text{intrinsic}} &= 2.5 \cdot \frac{N_A}{M} V_h \\
&= 2.5 \cdot \frac{N_A}{M} \cdot c_4 \left\langle R_g^3 \right\rangle \\
\eta_{\text{intrinsic}} &= 2.5 \cdot \frac{N_A}{M} \cdot c_4 \cdot c_5 \cdot L_k^{\frac{3}{2}}
\end{aligned} \tag{35}$$

Equation (35) shows that the intrinsic viscosity of DPS depends on Kuhn length.

3.2.4 Dynamic Viscosity

Pastor [8] discussed multiple extrapolation methods to calculate the intrinsic viscosity from dynamic viscosity in DPS. In the paper, the author [8] made comparison between the five methods which are shown in Equation (36-40) and finally recommended method C which is shown in Equation (38). The following equations can be used to determine the intrinsic viscosity of DPS experimentally.

A. Huggins equation(Huggins, 1942):

$$\frac{\eta_{\text{sp}}}{C} = \eta_{\text{intrinsic}} + k'\eta_{\text{intrinsic}}C \tag{36}$$

B. Kraemer equation(kraemer,1938):

$$\frac{\ln \eta_{rel}}{C} = \eta_{intrinsic} + k''\eta_{intrinsic}^{2}C \tag{37}$$

C. Simple viscosity model (Mcmillan,1974):

$$\eta_{rel} = 1 + \eta_{\text{intrinsic}}C \tag{38}$$

D. Exponential viscosity model

$$\eta_{rel} = e^{\eta_{\text{intrinsic}} \cdot C} \tag{39}$$

E. Inverse viscosity model

$$\eta_{rel} = \frac{1}{1 - \eta_{\text{intrinsic}} \cdot C} \tag{40}$$

Where η_{rel} and η_{sp} are as follows:

$$\eta_{rel} = \frac{\eta_{solution}}{\eta_{solvent}} \tag{41}$$

$$\eta_{sp} = \frac{\eta_{solution}}{\eta_{solvent}} - 1 \tag{42}$$

Where C is the concentration, and k' and k" are constantswhich can be determined experimentally.

From Equation (38), the viscosity of the solution can also be represented by the intrinsic viscosity in Equation (43).

$$\eta_{solution} = \left(1 + \eta_{\text{intrinsic}} \cdot C\right) \cdot \eta_{solvent} \tag{43}$$

3.2.5 Rigidity Effect on Dynamic Viscosity

To take into account the effect of polymer rigidity on dynamic viscosity of a DPS, the relationship between polymer Kuhn length and viscosity has been postulated explicitly as

shown in Equation (35). However, many dilute polymer solutions behave as non-Newtonian fluids, therefore, Equation (35) should be revised so it can be used in non-Newtonian DPS as explained in later in the chapter. One way to estimate the viscosity of DPS with different levels of polymer rigidity is by explicitly taking into account the relationship between polymer rigidity and Kuhn length or end-to-end vector ratio between polymers with same molecular weight as follows:

$$L_{k1} = m \cdot L_{k0} \tag{44}$$

$$\left\langle R_1^2 \right\rangle = m \left\langle R_0^2 \right\rangle \tag{45}$$

Where L_{k0}, L_{k1} are the Kuhn length of two polymers, m is the ratio of the Kuhn lengths between two polymers with identical molecular weight but with different rigidity. *m* can be defined as the rigidity changing parameter (RCP) in DPS. Equation 44 is based on the assumption that the Kuhn length is directly proportional to the level of rigidity of the polymer as expressed in Equation 13. It is also assumed that the Kuhn length of a polymer chain can be changed or adjusted by changing its chemical structure, CS (eg. make the

carbon chain into benzene ring)without changing its molecular weight (MW) or chemical composition, CC (i.e. $C_{35}H_{49}O_{29}$).

By finding the intrinsic viscosity ratio between two DPS made of polymers with the same MW or CC but with different CS based on Equation (35), the viscosity values of less or more rigid DPS can be found directly using Equation (44).

$$\frac{\eta_{intrinsic\,1}}{\eta_{intrinsic\,0}} = \frac{L_1^{\frac{3}{2}}}{L_0^{\frac{3}{2}}} = \left(\frac{L_1}{L_0}\right)^{\frac{3}{2}} = m^{\frac{3}{2}} \tag{46}$$

By combining equations (38) and (44), the following Equation can be obtained (47):

$$\frac{\eta_{\text{intrinsic 1}}}{\eta_{\text{intrinsic 0}}} = m^{\frac{3}{2}}$$

$$\frac{\eta_{\text{intrinsic 1}}}{\eta_{\text{intrinsic 0}}} = \frac{\left(\frac{\eta_{\text{solution 1}} - \eta_{solvent}}{\eta_{solvent} \cdot C}\right)}{\left(\frac{\eta_{\text{solution 0}} - \eta_{solvent}}{\eta_{solvent} \cdot C}\right)} \tag{47}$$

Solving for $\eta_{solution1}$, a viscosity model for DPS is as follows

$$\eta_{solution1} = \left[\left(\frac{\eta_{solution0} - \eta_{solvent}}{\eta_{solvent} \cdot C} \right) \cdot m^{\frac{3}{2}} \cdot C + 1 \right] \cdot \eta_{solvent} \qquad (48)$$
$$= (\eta_0 - \eta_{solvent}) \cdot m^{\frac{3}{2}} + \eta_{solvent}$$

3.2.6 Viscosity of Xanthan Solution

For simulation purposes, the viscosity of 0.2% xanthan solution was used due to the availability of experimental data both in terms of rigidity and viscosity. Furthermore, a dilute xanthan solutions follows the classic power law model since it behaves as a non-Newtonian fluid. Experiments and numerical analysis of dilute xanthan solutions have already been undertaken by Pastor [8] so complete knowledge of the flow and consistency index data are available. The viscosity and the rigidities were taken into account by using Equation (2) and Equation (48), and were shown in equation (49).

$$\eta = \left(0.64\dot{\gamma}^{-0.69} - \eta_{solvent} \right) \cdot m^{\frac{3}{2}} + \eta_{solvent} \qquad (49)$$

Where m is the RCP and is the dynamic viscosity of DPS with certain rigidity.

3.3 Boundary Condition

Several boundary conditions were defined and used in the study. Two different initial velocities of the flow were taken into account. The inlet flow velocity profile was assumed to uniform as in plug flow cases. The wall was heated with constant surface heat flux 100 W/m^2.

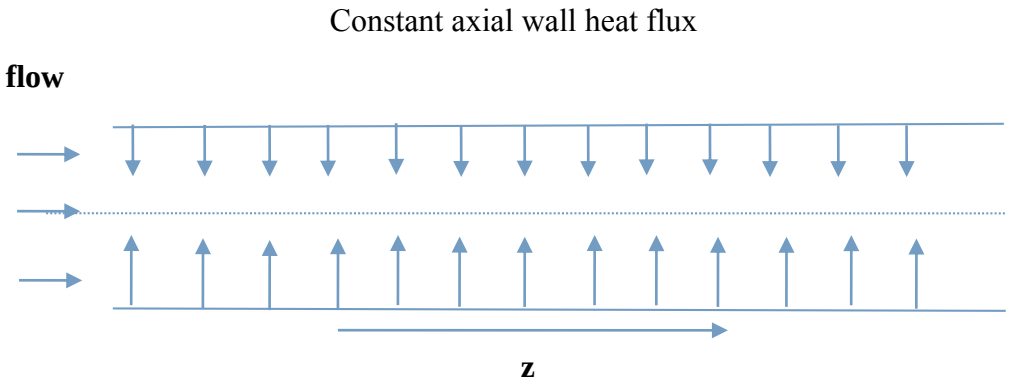

Fig. 3.3 Uniform wall heat flux in circular pipe

3.4 Materials

In the study, dilute xanthan solutions with concentration of 0.2% were chosen for analysis and simulation due to the availability of viscosity data [8].

3.5 Rheological and Heat Transfer Parameters

Several parameters were identified and selected for the study. The following subsections outlines the parameters chosen for simulation and analysis purposes.

3.5.1 Reynolds Number

The Reynolds number is defined as the ratio of the inertial force to the viscous force of the flow, and it is a dimensionless parameter which can be utilized to characterize different flow regions, such as laminar flow and turbulent flow. For Newtonian fluid the Reynolds number is defined in Equation (50):

$$\mathrm{Re} = \frac{\rho U_m D_h}{\mu_{\mathrm{eff}}} \tag{50}$$

Where ρ is the density of the fluid, U_m is the mean velocity, D_h is the hydraulic diameter, μ is the dynamic viscosity of the fluid.

For Non-Newtonian fluid the Reynolds number cannot be calculated by Equation (50) due to the changing viscosities of non-Newtonian flow. The general equation of Reynolds number for non-Newtonian fluids based on the Power Law model is given in equation (51):

$$\mathrm{Re} = 2^{3\text{-}n}\left(\frac{n}{3n+1}\right)^n \frac{\overline{V}^{2-n} D^n \rho}{K} \tag{51}$$

Where n is the flow index of the power law fluid, $\overline{V}$ is the area average velocity, D is the hydraulic diameter, and ρ is the density of power law fluid.

3.5.2 Grashof Number

The Grashof number (Gr) is a dimensionless parameter that used to approximate the ratio of the buoyancy to the viscous forces on a fluid [41]. If $Gr<<Re^2$, forced convection is considered to be the main effect on heat transfer of the fluid, and natural convection can be neglected. To the contrary if $Gr >> Re^2$, forced convection can be neglected. When $Gr \approx Re^2$, then both forced convection and natural convection should be taken into account since they have similar influence on heat transfer. The Grashof number for power law Non-Newtonian fluid is given in equation (52):

$$Gr = \frac{\beta \Delta T D^3 \rho^2 g}{\mu_{eff}^2} \tag{52}$$

Where β is the volumetric thermal expansion coefficient, ΔT is the temperature difference between the surface temperature and the bulk temperature. D is the diameter of the pipe, ρ is the density of the fluid, g is acceleration due to Earth's gravity, μ_{eff} is the effective viscosity at the wall shear rate and temperature.

3.5.3 Density

The density of the polymer solution is determined by Equation (53). It is obtained by the volume averaged density of the individual components of the solution.

$$\rho_s = c\rho_x + (1-c)\rho_0 \tag{53}$$

Where ρ_s is the density of the polymer solution, $\rho_x$is the density of xanthan, $\rho_0$is the density of the solvent, c is the solute concentration.

3.5.4 Polymer Rigidity

To study the influence of polymer rigidity on the viscosity of the DPS, the rigidity parameter m has been introduced above to describe the rigidity difference between different DPS. The introduction of m has been discussed in 3.2.4.

3.5.5 Thermal Conductivity

In the case of dilute polymer solution, the mass concentration of polymer molecules is 0.2%. To simplify the problem the thermal conductivity of dilute polymer solution was considered to be constant and the same as the thermal conductivity of the solvent.

3.5.6 Specific Heat

The specific heat of DPS was determined using equation (54). Because of the low concentration, the specific heat of polymer solution can be simplified and assumed to be the same with the specific heat of the solvent.

$$C_{ps} = cC_{px} + (1-c)C_{p0} \tag{54}$$

Where C_{ps} is the specific heat of the polymer solution, C_{px} is the specific heat of xanthan, C_{p0} is the specific heat of the solvent.

3.5.7 Velocity Profile

In the case of non-Newtonian laminar flow in smooth circular pipe, the fully developed velocity profile was obtained from Skelland [2]. The velocity profile can be generally expressed by equation (55).

$$\mathrm{V_r} = \frac{3n+1}{n+1} \cdot U \cdot \left[1 - \left(\frac{r}{R} \right)^{\frac{n+1}{n}} \right] \tag{55}$$

Where V_r is the velocity on radial position, r is the distance from the specific point to the center in radial direction. R is the radius of the pipe, U is the mean velocity, n is the flow index of the power law fluid.

3.5.8 Graetz Number

The Graetz number (Gz) is a dimensionless parameter that can be used to characterize laminar flow in a pipe. The Graetz number is given in equation (56):

$$Gz = \frac{\dot{m}C_p}{kL} \tag{56}$$

Where $\dot{m}$ is the mass flow rate of the fluid, C_p is the specific heat, k is the consistency index, L is the length of the tube.

3.5.9 Nusselt Number

Nusselt number is a dimensionless parameter that can be utilized to measure the convection heat transfer at a boundary within fluids. The theoretical solution of the Nusselt number for the power law fluid laminar flow under the boundary condition of the constant wall heat flux is given by equation (57):

$$Nu = 1.42\left(\frac{3n+1}{4n}\right)^{\frac{1}{3}} \cdot Gz^{\frac{1}{3}} \tag{57}$$

Where *Gz* is the Graetz number, *n* is the flow index of the power law model. Equation [1] is for the situation that the flow has a Graetz number larger than 100 but smaller than 10000.

For simulation purposes, the Nusselt number was calculated directly from the simulation results, using equation (58).

$$Nu = \frac{h \cdot l}{k}$$
$$Nu = \frac{q'' \cdot l}{(T_w - T_b) \cdot k} \tag{58}$$

Where *h* is the convective heat transfer coefficient of the fluid, q'' is the heat flux, *l* is the characteristic length.

3.5.10 Friction Factor

In fluid dynamics, the friction factor is a dimensionless parameter which relates the pressure drop to the kinetic energy of the fluid. It can be calculated from the shear stress at the wall. The friction factor is given in equation (59).

$$C_f = \frac{\tau_w}{\rho U_0^2 / 2} \tag{59}$$

Where $C_f$is the fanning friction factor, ρ is the density of the fluid, U_0 is the inlet velocity, $\tau_w$is the wall shear stress, which can be obtained by applying equation (60).

$$\tau_w = \dot{\gamma}_w \cdot \eta \tag{60}$$

Where η is the viscosity of the solution, $\dot{\gamma}_w$ is the shear rate along the wall, which can be numerically obtained from Fluent by using the radial velocity and equation (61)

$$\dot{\gamma}_w = \frac{V_l - V_w}{l} \tag{61}$$

Where V_l is the velocity of the nearest grid to the wall, and l is the distance between the wall and the grid in radial direction. V_w is zero because of the non-slip condition.

In hydrodynamically fully developed region, the fanning friction factor can be obtained for laminar flow from known Reynolds number as follows:

$$f = \frac{16}{\mathrm{Re}} \tag{62}$$

3.6 Modeling Procedure

In order to model the thermal behavior of non-Newtonian fluids computationally, a detailed modeling procedure was developed as shown in Fig. 3.4. The modeling procedure is based on standard heat transfer modeling with the classic circular pipe meshed by a mesh generator. The boundary conditions were imposed to get stable numerical results, and comparisons were made between simulation results and theoretical results.

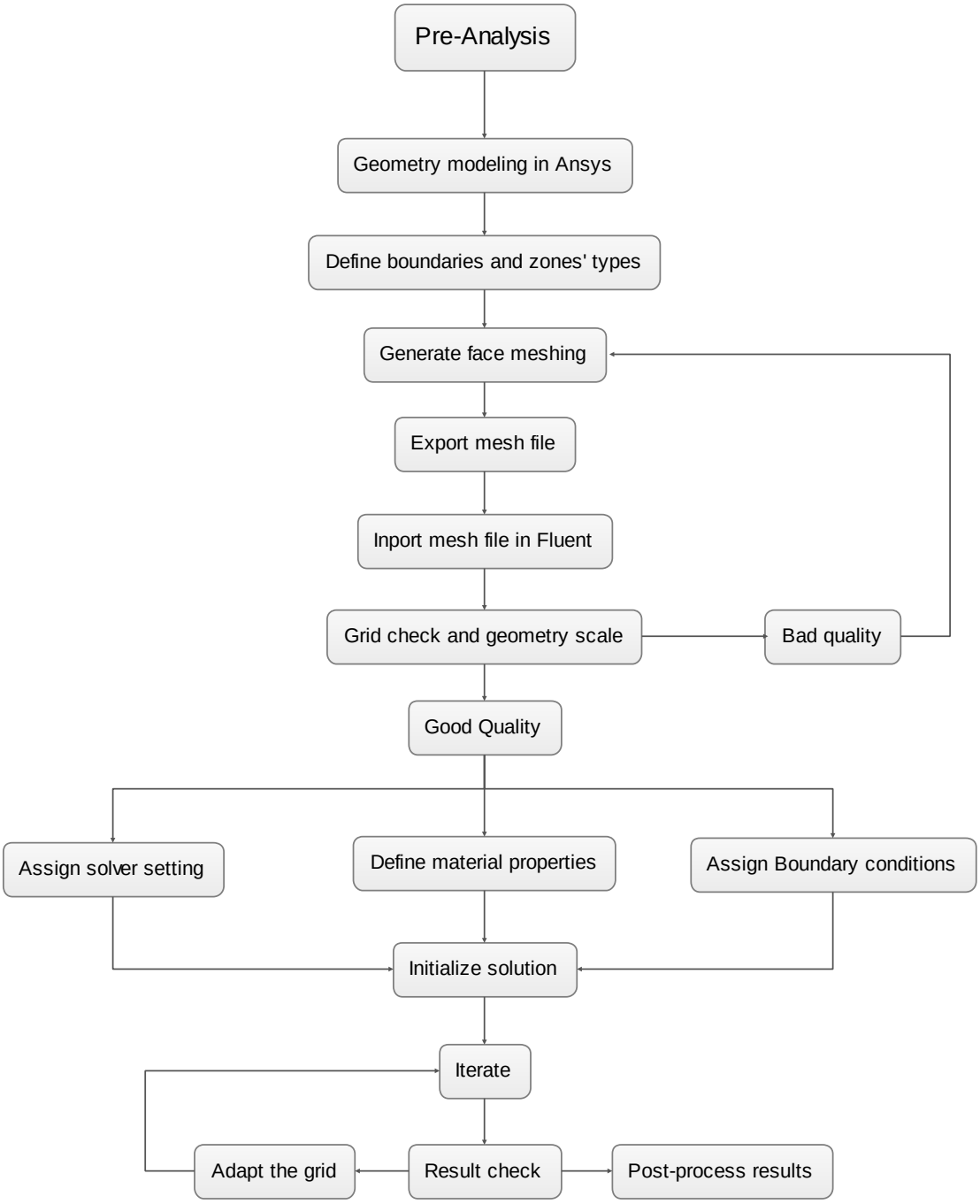

Fig. 3.4 Modeling and solution procedure

3.7 Grid Generation Techniques

A basic geometry was selected for the study. The geometry consisted of 2-D smooth circular tube, with inlet, outlet, wall, and an axis. Several mesh structures were considered and tested using simple boundary conditions. The results of simulation were used to determine which meshing model could provide the most accurate results both in the cases of friction factor and Nusselt number. The simulations were undertaken and solved based on an axis-symmetric method [39], which converts the 2D system into a 3D configuration by assuming perfect symmetry along the axial distance. Since the mesh quality is determined by the orthogonal quality and the aspect ratio, the size and shape for each mesh cell should be controlled and adjusted to obtain reliable results. The best shape for 2-D mesh cell is the square, thus the length and the width of each cell were set to be the same. Different mesh densities were utilized to optimize the simulation and the results of Nusselt number were compared with theoretical solutions. It was found the error for Nusselt number was less than 1% once the number of mesh grids was greater than 200,000. Thus for a 0.01m diameter and 0.5m long pipe, the axial distance was divided into 5000 elements, and the radial distance was divided into 100 elements. As a result, the final mesh density was $5*10^5$ grids. The mesh distribution is shown in Fig.3.3, and the minimum orthogonal quality was 1 with a maximum aspect ratio is 1.416.

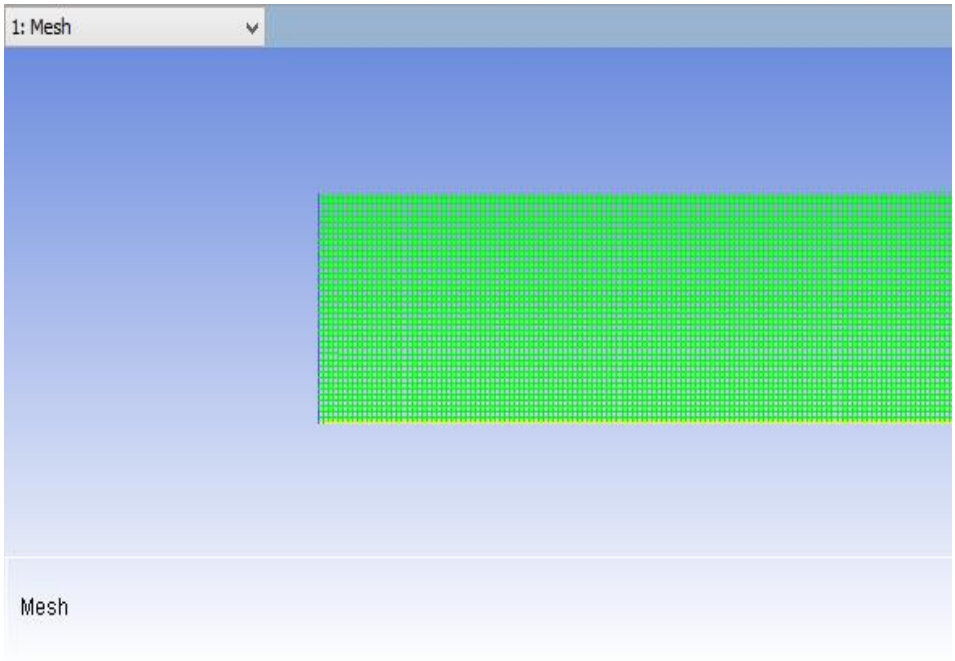

Fig. 3.5 Mesh distribution of geometry

3.8 Modeling Using FLUENT 14.0

The heat transfer of non-Newtonian flow in circular pipe with uniform heat flux was solved as a two dimensional problem with a double precision solver. GAMBIT, a commercial mesh generating software was utilized to create the geometry and mesh model for analysis in FLUENT 14.0. The default (0.5) under relaxation factors provided in FLUENT 14.0 was used for momentum, pressure, and energy calculations. A second order discretization scheme was used to solve pressure, energy and momentum of the PCM fluid.

The SIMPLE pressure-velocity coupling algorithm was used to derive equations for pressure from the discrete continuity equation.

A plug velocity profile was set as initial boundary condition at the inlet of the tube, and the problem was solved by assuming a hydro-dynamically developing and thermally developing flow. The convergence criterion for the continuity, momentum and energy equations was set to 10^{-12}. During post processing, Fluent was used to determine the wall temperatures, the mass weighted average temperature and the velocity profiles. These values were used to calculate the local Nusselt number, the friction factor and the Reynolds number.

RESULTS AND DISCUSSION

This chapter includes numerical simulation results for Newtonian and non-Newtonian heat transfer fluids under constant heat flux conditions. The first section deals with validation of the numerical scheme and grid use in the study. The latter sections show simulation results for DPS fluids.

4.1 Numerical Validation

The numerical simulations were undertaken using water as the heat transfer fluid. The numerical solutions have been compared with experimental, analytical and previous numerical results in this section.

Fig. (4.1) shows a dimensionless fully developed velocity profile for a classic Newtonian fluid (water) in a circular pipe with constant wall heat flux condition. The Reynolds number in fully developed region was set to 1000, and the results from the simulations agreed within 1% of the theoretical results for laminar flow. The fully developed velocity profile was utilized to study the heat transfer performance of a circular pipe under laminar conditions, and the numerically-obtained local Nusselt number was

validated using the theoretical Nusselt number equation [11] for water under constant wall heat flux boundary condition. The error was within 1% of the analytical solution and the results are shown in Fig 4.2.

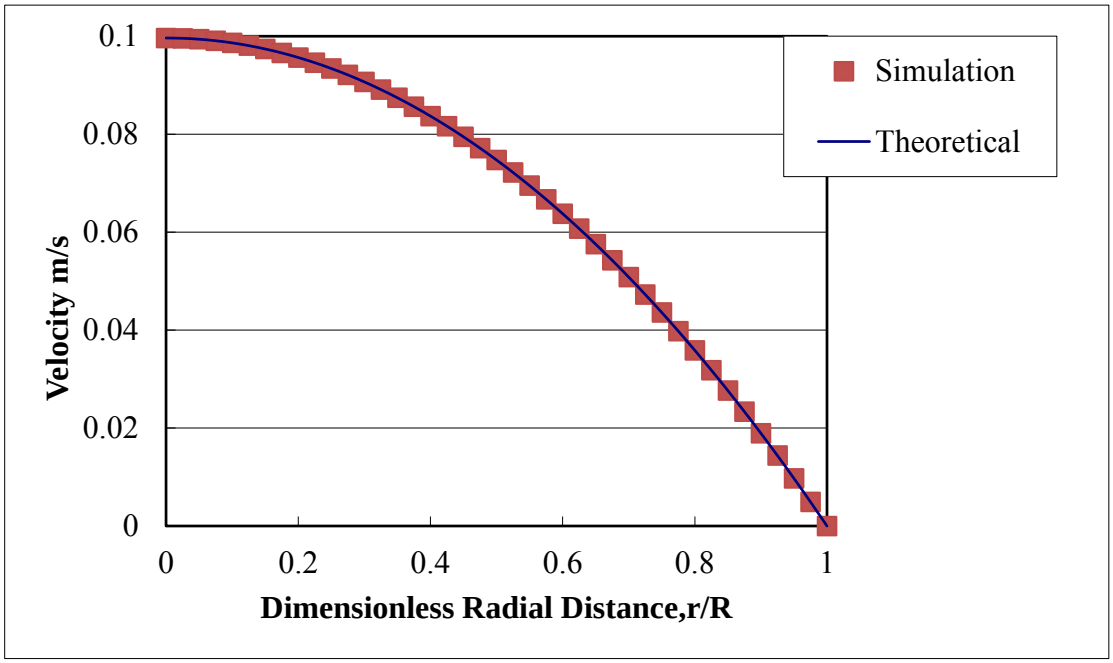

Fig. 4.1 Dimensionless fully developed velocity profile

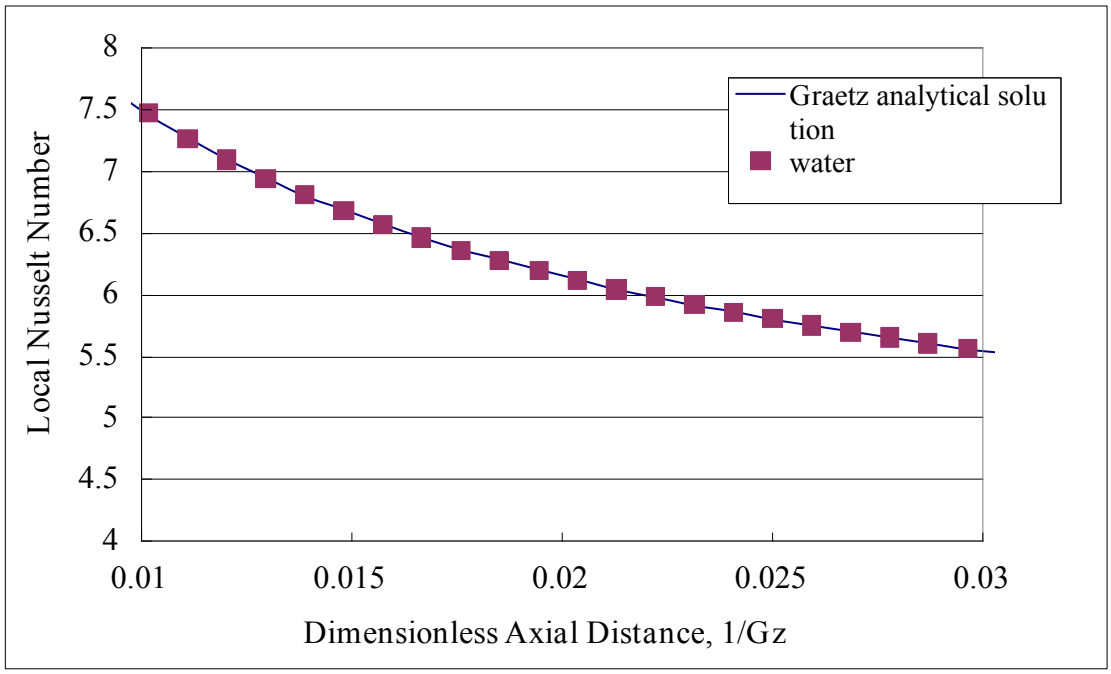

Fig. 4.2 Local Nusselt number of water

Then the analysis of a non-Newtonian power law fluid, 0.2% xanthan solution, was undertaken using a two dimensional geometry model for a smooth circular pipe. The viscosity of the power law fluid [8] is given in equation (63).

$$\eta = 0.64 \cdot \dot{\gamma}^{-0.69} \tag{63}$$

The Reynolds (Re) number in hydro-dynamically fully developed region was set to 10.76, the Grashof (Gr) number of this case was 2.24, so the ratio of Re^2/Gr was 51.3, which is much larger than 1, thus the natural convection was considered to be negligible.

The fully developed velocity profile for a non-Newtonian power law fluid was compared with known theoretical velocity profile obtained using Equation 53. The results are shown in Fig. 4.3. A plug flow inlet velocity profile was utilized to determine the friction factor and the heat transfer performance of a circular tube under laminar flow conditions. The numerical-obtained Nusselt number (Nu) for this case was validated with known theoretical solution of Nusselt number (Nu) under constant heat flux in circular smooth pipe. The numerical result of Nusselt number (Nu) agreed within 2% of the analytical results and the comparisons are shown in Fig. 4.4.

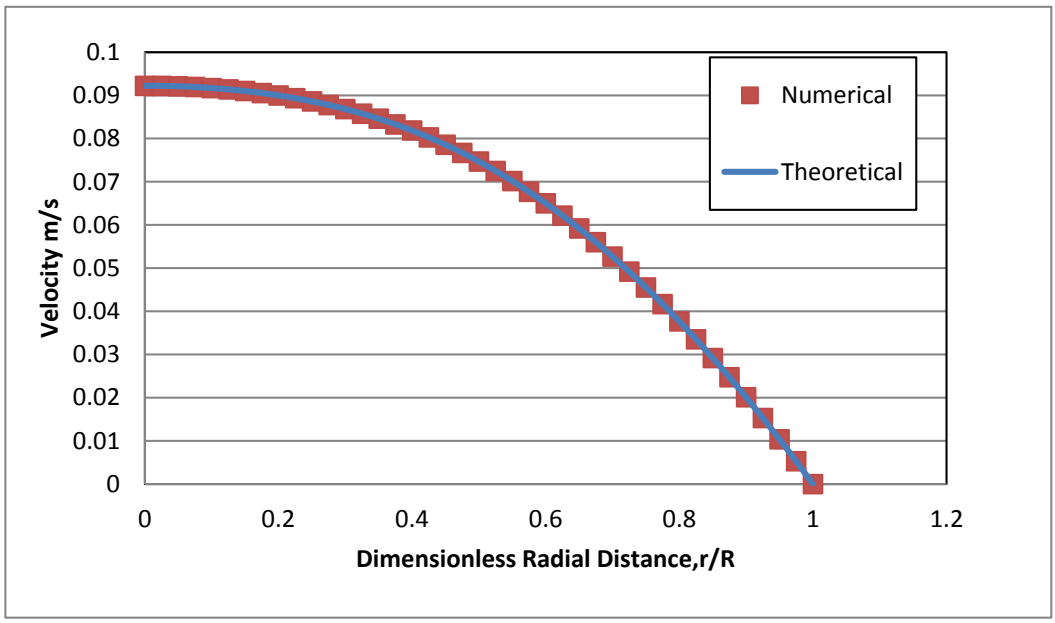

Fig. 4.3 Velocity profile of power law fluid

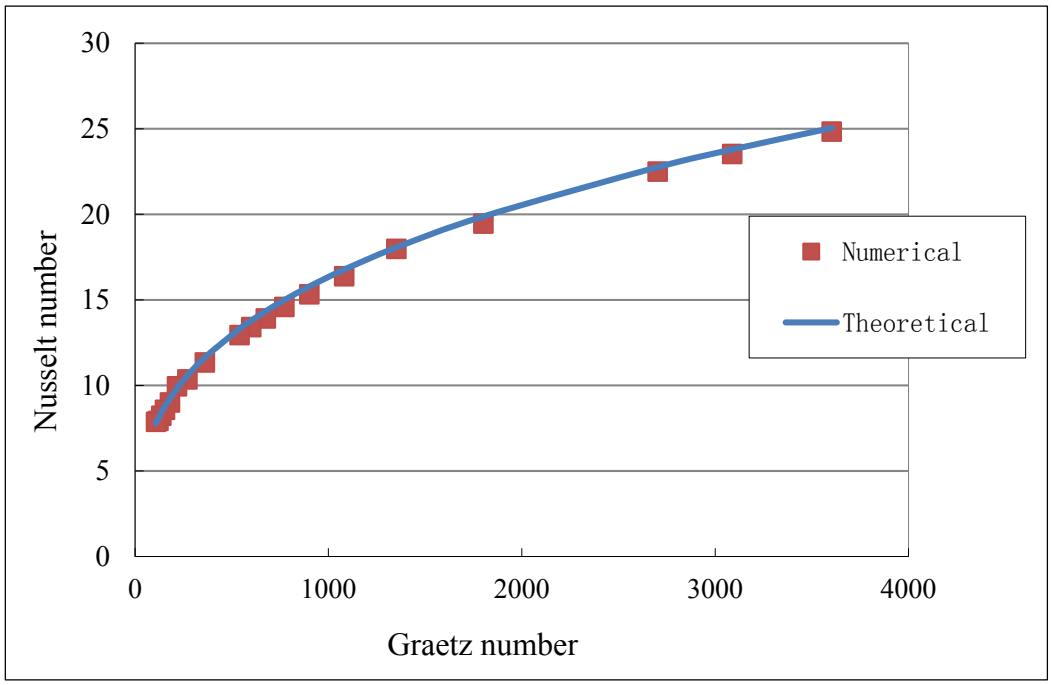

Fig. 4.4 Local Nusselt number of power law fluid

With the fully developed velocity profile, the fanning friction factor was obtained and shown in Fig.4.5.

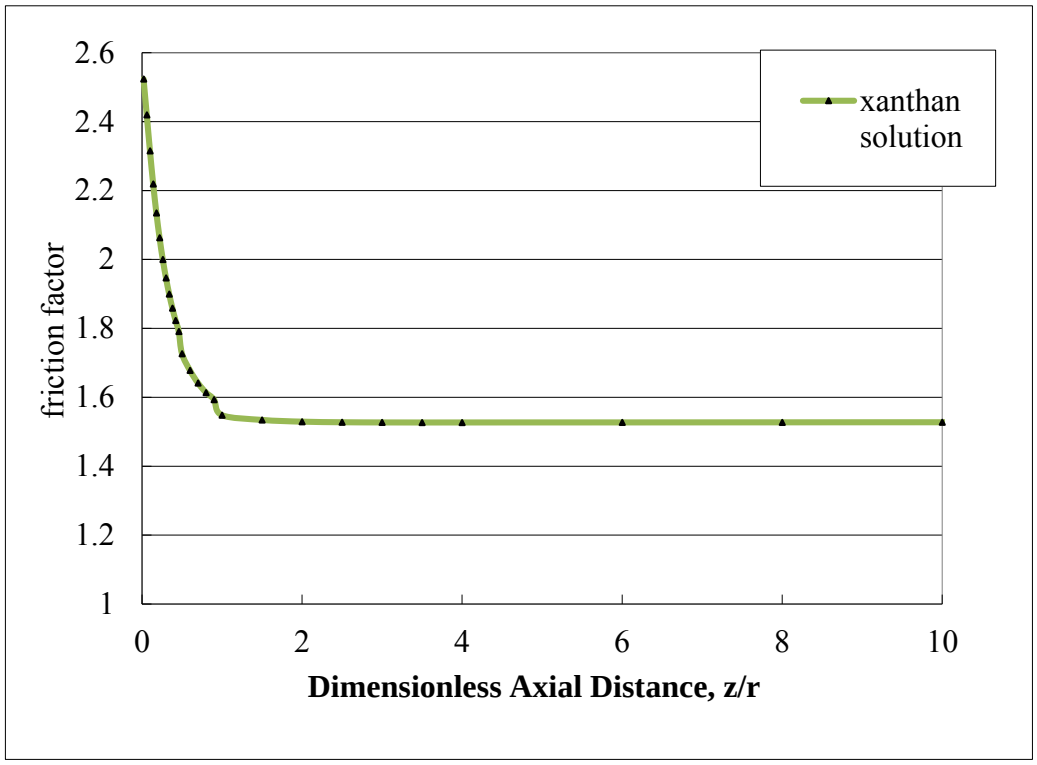

Fig. 4.5 Friction factor of 0.2% xanthan solution with inlet velocity 0.05m/s

It can be observed that in hydro-dynamically developing region, the friction factor decreases. In hydro-dynamically fully developed region, the friction factor reaches a steady state value of 1.52, which compares well with the theoretical solution which is 1.49, giving an error of 2%.

4.2 Power Law Fluid in Circular Pipe

Two cases of non-Newtonian flow with two different initial velocities were studied and the heat transfer performance of the power law flow in circular pipe with constant wall heat flux condition are discussed in this section.

To study the effect of polymer rigidity on the behavior of DPS, 0.2% xanthan solution was set as the baseline for parametric analysis. Different rigidity changing parameters (RCP) or *m* values were used as shown in Table 1.

DPS Name	**RCP (*m*)**	**Rigidity compared with 0.2% xanthan DPS**
Sample 1	0.5	Flexible
Sample 2	0.75	Flexible
0.2% xanthan solution	1	Baseline sample
Sample 3	2	Rigid

Table 1. Rigidity changing parameter of DPS

By choosing the value of *m*, the viscosities for these four DPS was calculated using equation (49) which was introduced in section 3.2.6, shown in Table 2.

Rigidity Parameter (m)	Viscosity of DPS (power law fluid)
m	$\eta_{\text{solution 1}} = \left(k\dot{\gamma}^{n-1} - \eta_{solvent}\right)\cdot m^{3/2} + \eta_{solvent}$
0.5	$\eta = 0.5^{3/2}\cdot\left(0.64\dot{\gamma}^{-0.69}\right) + \left(1\text{-}0.5^{3/2}\right)\cdot\eta_{\text{water}}$
0.75	$\eta = 0.75^{3/2}\cdot 0.64\dot{\gamma}^{-0.69} + (1\text{-}0.75^{3/2})\cdot\eta_{\text{water}}$
1	$\eta = 0.64\dot{\gamma}^{-0.69}$
2	$\eta = 0.75^{3/2}\cdot 0.64\dot{\gamma}^{-0.69} + (1\text{-}0.75^{3/2})\cdot\eta_{\text{water}}$

Table 2. Viscosity of DPS at various rigidity levels

Two simulation cases were considered. Case 1 had an inlet velocity of 0.05 m/s , while Case 2 had an inlet velocity of 0.1m/s.

The boundary conditions were carefully set in order to ensure turbulent flow and natural convection were negligible. To better control the flow conditions, the Reynolds numbers were carefully controlled and the Grashof numbers were calculated to make numerical comparisons with the square of Reynolds number. The Reynolds number could be found once the inlet velocity was chosen. Table 3 and Table fig4 show flow conditions for inlet velocity of DPS at 0.05 and 0.1 m/sec, respectively are the Case 1 and Case 2.

Rigidity	U_0	Re	Gr	Re^2	Re^2/Gr
m=0.5	0.05m/s	30.48	17.92	929	51.8
m=0.75	0.05m/s	16.57	5.32	274	51.5
m=1	0.05m/s	10.76	2.24	115	51.3
m=2	0.05m/s	3.81	0.28	15	53.5

Table 3. Case1: Flow conditions at inlet velocity of 0.05 m/sec

Rigidity	U_0	Re	Gr	Re^2	Re^2/Gr
m=0.5	0.1m/s	98.24	25.29	9651	381.6
m=0.75	0.1m/s	53.48	7.495	2861	381.7
m=1	0.1m/s	34.73	3.162	1206	381.6
m=2	0.1m/s	12.28	0.395	150	381.5

Table 4. Case 2: Flow conditions at inlet velocity of 0.1 m/sec

Where U_0 is the inlet velocity, Re is the Reynolds number and Gr is the Grashof number. As it can be seen, the ratio between Re^2 and Gr is much bigger than 1 in all the cases, which indicates that the effect of natural convection in the cases can be negligible and neglected.

Fig.4.6 shows the fully developed velocity profile for 0.2% xanthan solution compared with water. It can be observed that the velocity profile for the non-Newtonian (xanthan DPS) is flatter than that of water.

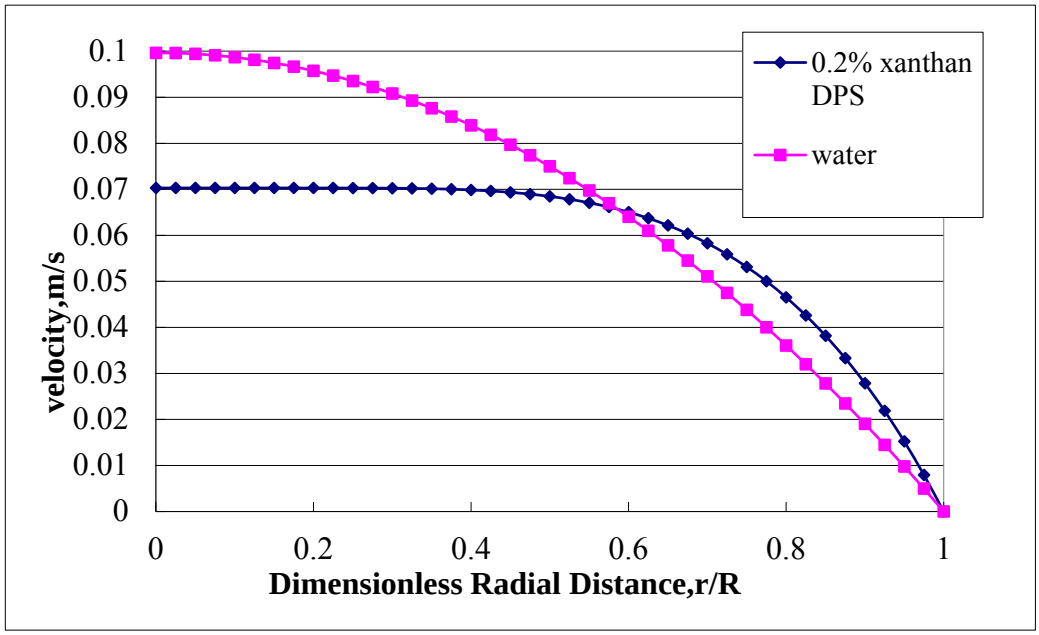

Fig. 4.6 Velocity profile of 0.2% xanthan DPS

In the hydro-dynamically developing region, the velocity profile for 0.2% xanthan DPS is shown in Fig.4.7. It can be seen that the velocity developed from an initial plug flow shape to a non-Newtonian power law shape when z/r increased from 0.1 to 2.5.

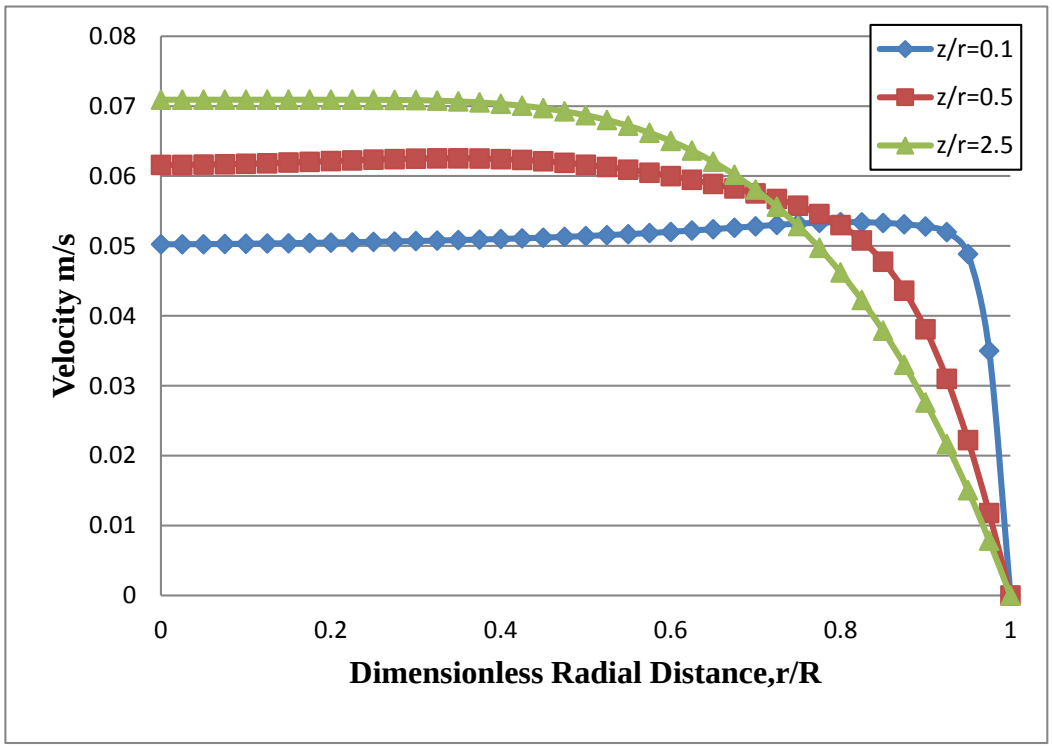

Fig. 4.7 Developing velocity profile of 0.2% xanthan solution

Fig.4.8 shows local Nusselt number along the axial direction of the pipe for Casen 1. Two close up figures of the same process can be seen in Fig.4.9 and Fig.4.10, which show the Nusselt number in the entrance region of the pipe and the tiny difference of Nusselt number near the hydro-dynamically fully developed region.

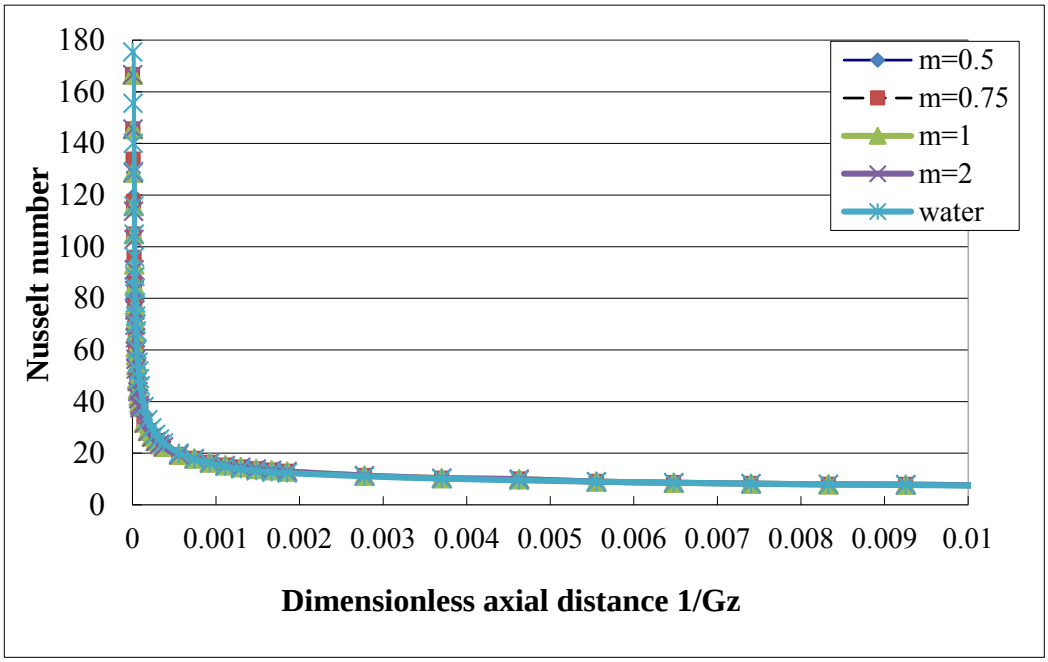

Fig. 4.8 Variation of Nu for power law fluid in Case 1

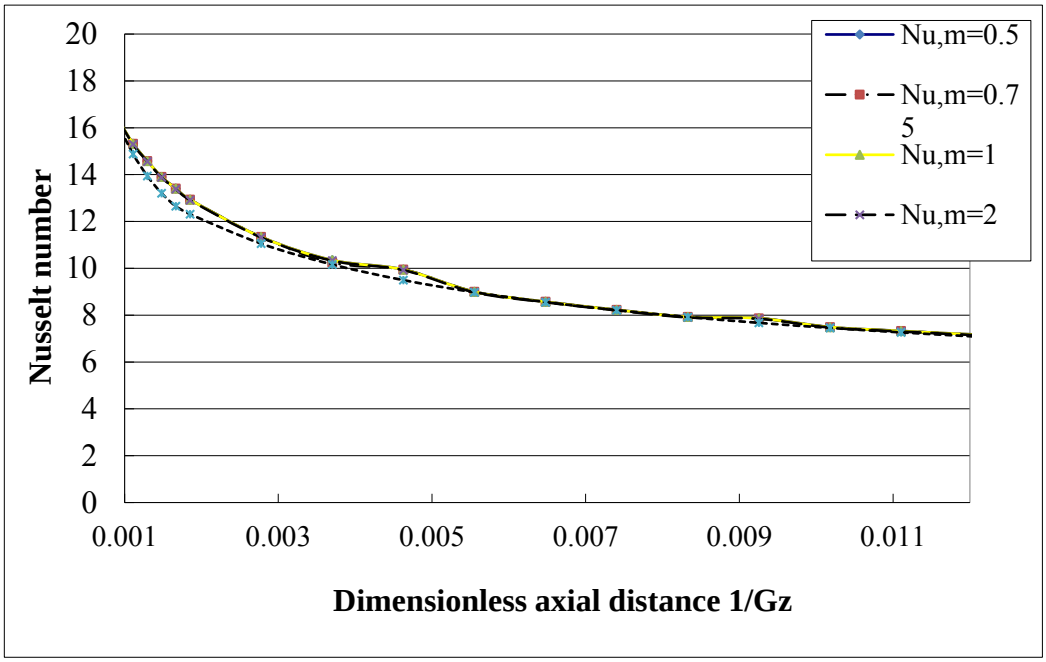

Fig. 4.9 Variation of Nu in the Gz^{-1} range of 0.001 to 0.011

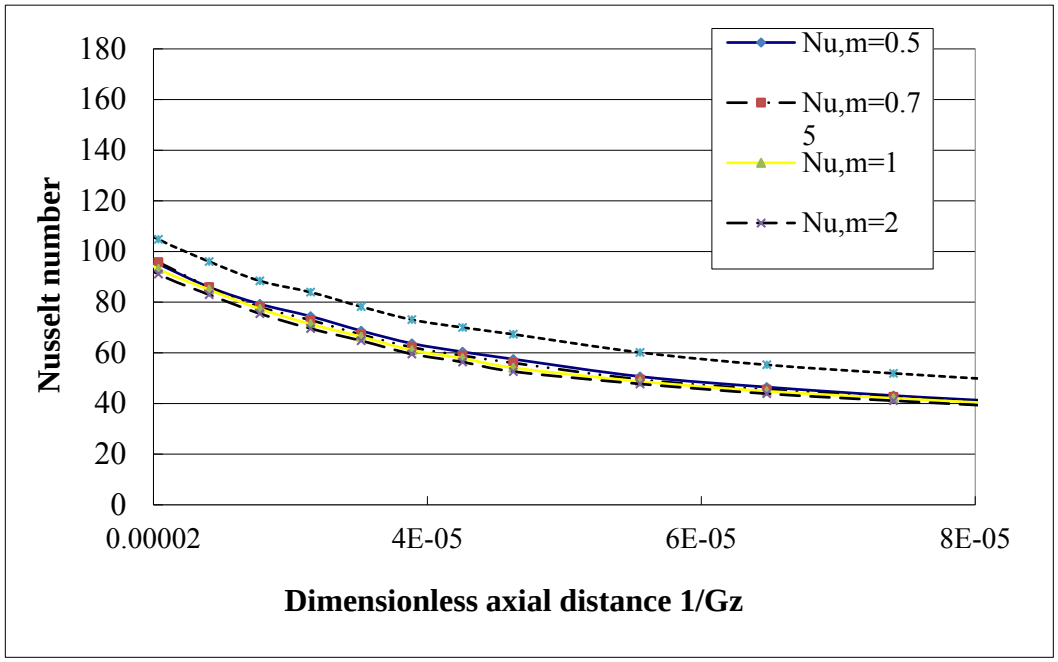

Fig. 4.10 Variation of Nu in the Gz^{-1} range of $2E^{-5}$ to $8E^{-5}$

In Fig (4.8-4.10) it can be seen that the Nusselt number for all DPS and water decreased as the value of Gz^{-1}increased, and the trend became more smooth when the value of 1/Gz was greater than 0.000004. In entrance region, the local Nusselt number decreases slightly when the DPS is more rigid ($m = 2$). Also the Nusselt number of water is higher than that of DPS. In hydro-dynamically fully developed region the local Nusselt number for DPS with different rigidities are similar with each other.

For case 2, the local Nusselt number is shown in Fig 4.11. Two close up figures for the entrance region and hydro-dynamically fully developed region can be seen in Fig.4.12 and Fig.4.13.

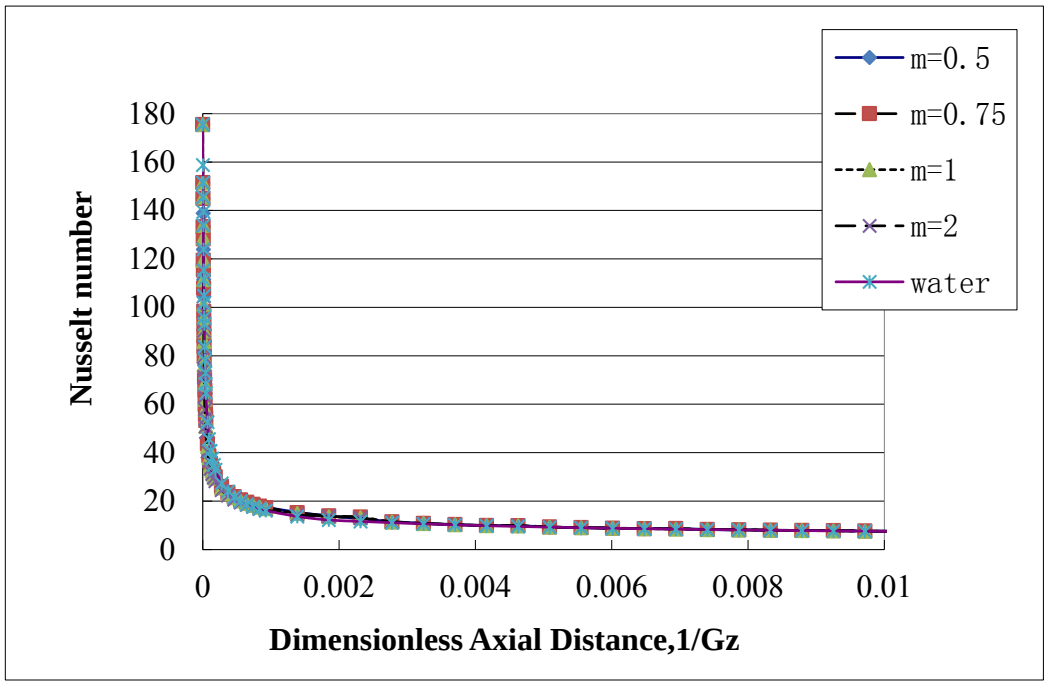

Fig. 4.11 Variation of Nu for power law fluid in Case 2

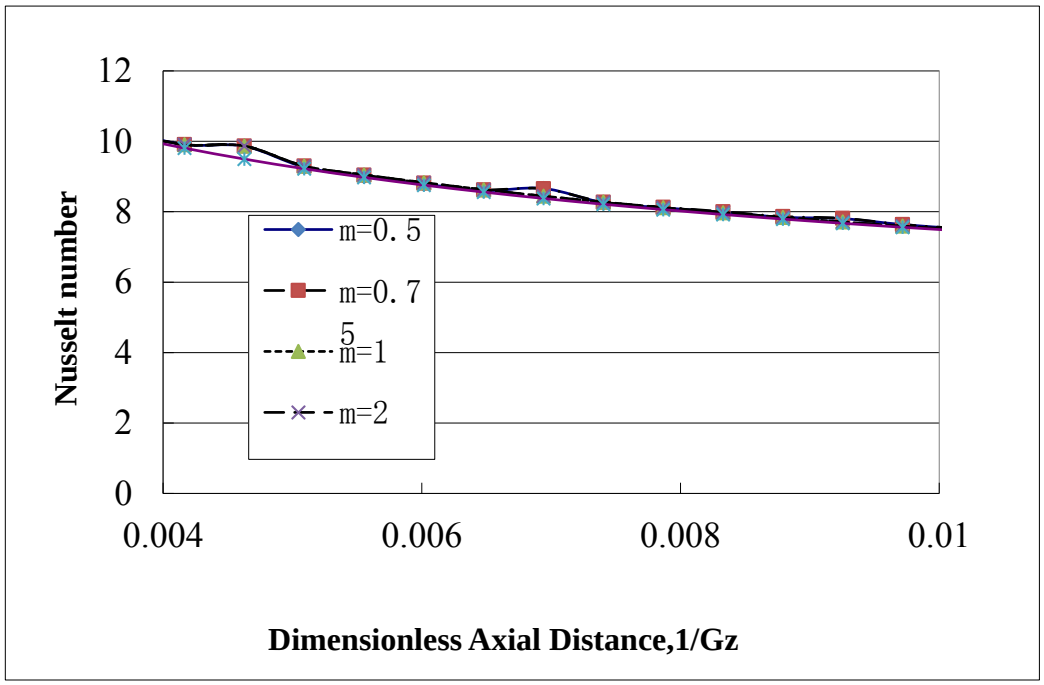

Fig. 4.12 Variation of Nu in the Gz^{-1} range of 0.004 to 0.01

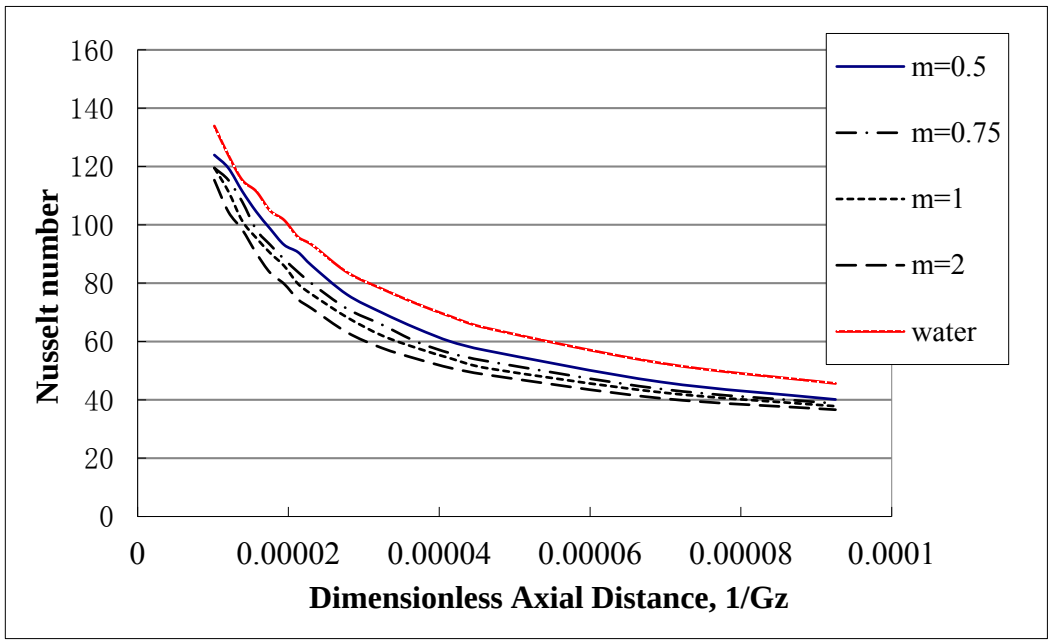

Fig. 4.13 Variation of Nu in the Gz^{-1} range of $2E^{-5}$ to $1e^{-4}$

In the hydro-dynamically developed region, it can be seen that the local Nusselt number of DPS was independent on the rigidity of polymer chain, and the Nusselt number of DPS converged to the same result which is numerically close to the Nusselt number of water. By studying the theoretical Nusselt number solution of power law fluid which is given in section 3.5.9, the Nusselt number was mainly affected by the Graetz number and the flow index. However, the rigidity model only takes into account the consistency, thus the Nusselt number does not vary much when the rigidity of the polymers in solution change as indicated in Table 2.

It can also be seen that in hydro-dynamically developing region, a more rigid DPS yields a slightly lower Nusselt number than that of a flexible DPS.

The friction factor curves of different DPS in Case 1 and water are shown in Fig.4.14, and close up friction factor curves for the developing region are given in Fig.4.15.

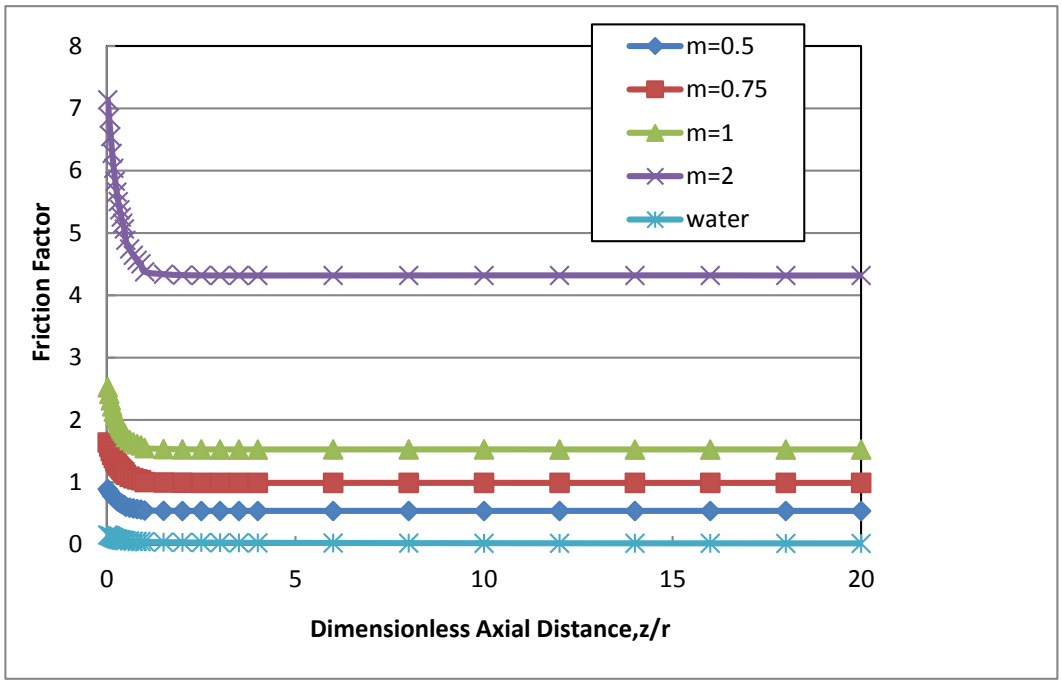

Fig. 4.14 Friction factor for Case 1

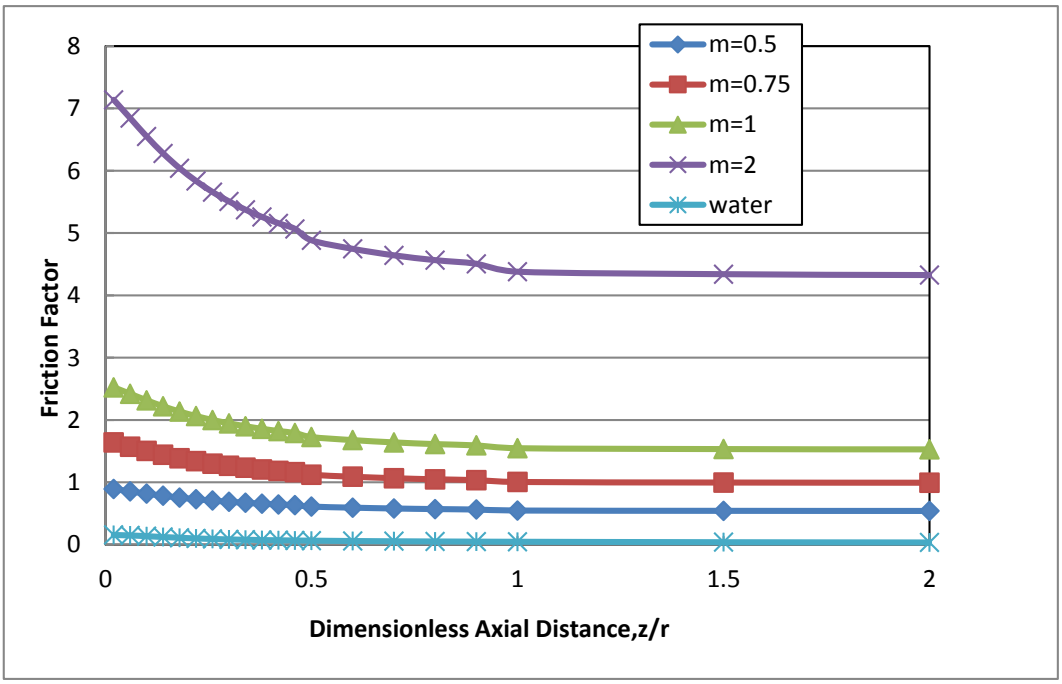

Fig. 4.15 Friction factor for Case 2

The friction factor curves of Case 2 for DPS and water are also presented in Fig.4.16 with a close up friction factor curves for hydro-dynamically developing region shown in Fig.4.17.

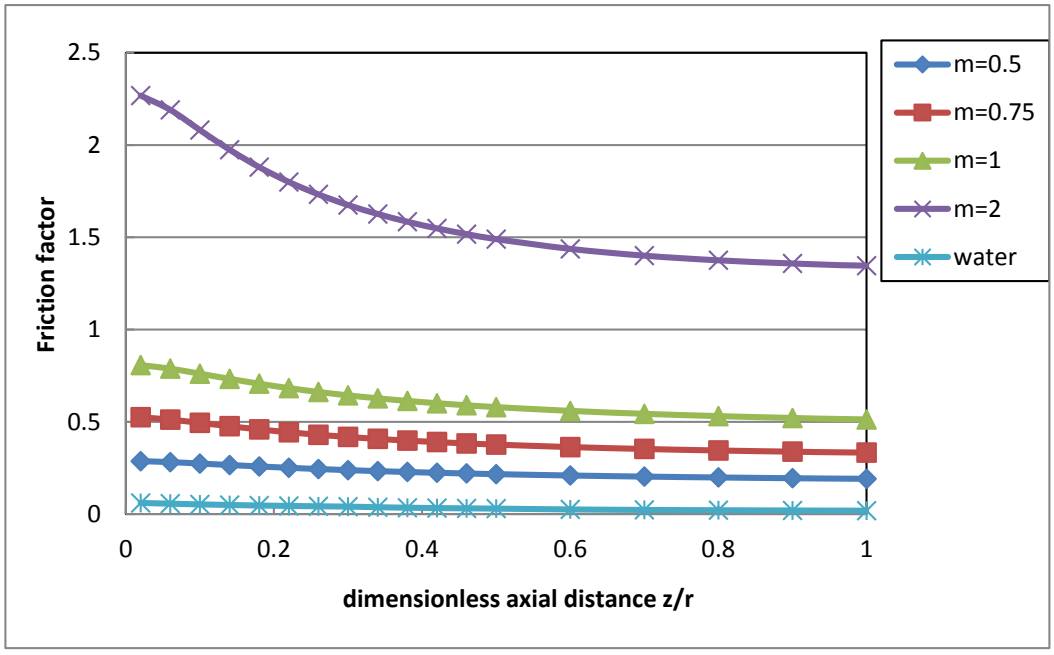

Fig. 4.16 Friction factor for Case 2 in dimensionless axial distance from 0 to 1

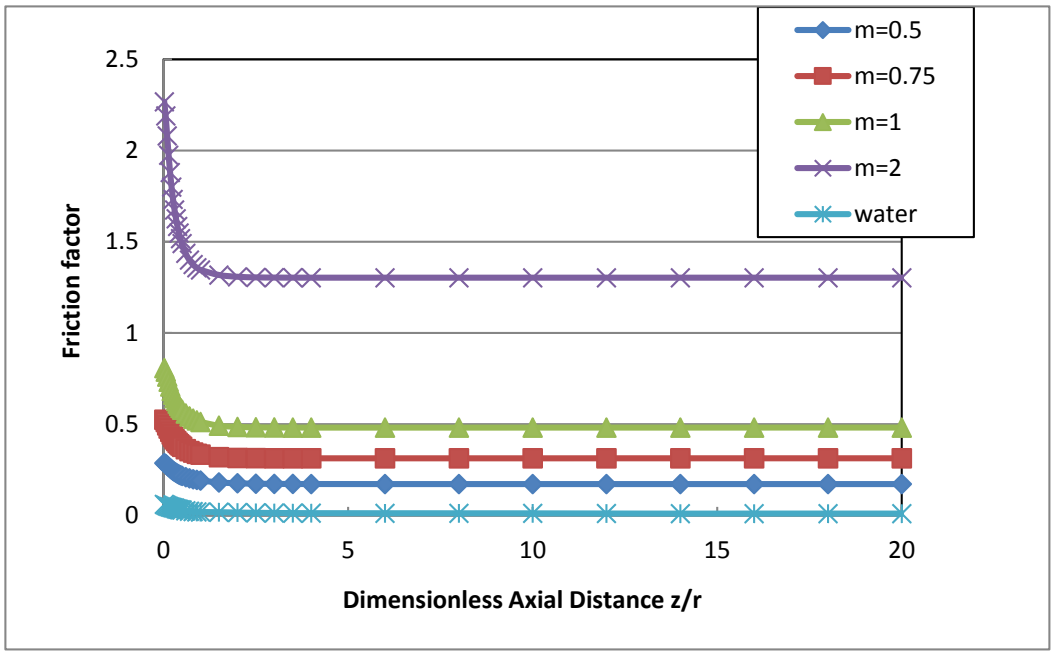

Fig. 4.17 Friction factor for Case 2

It can be seen that the effect of rigidity on the friction factors of DPS is significant. This is because the rigidity of DPS affects the viscosity of the solution, resulting in greater surface shear stress and friction losses when compared to water under laminar flow conditions. Furthermore, rigid DPS always have much larger friction factor than the flexible DPS.

The performance evaluation criteria (PEC), which is defined in Equation (64) was also evaluated for Case 1 and Case 2.

$$PEC = \left(\frac{\left(\frac{Nu_{sample}}{Nu_{water}} \right)}{\left(\frac{f_{sample}}{f_{water}} \right)^{1/3}} \right) \tag{64}$$

Where Nu_{sample} is the local Nusselt number of tested fluid, Nu_{water} is the local Nusselt number of water with the same boundary condition as tested fluid, f_{sample} is the friction factor of tested sample, and f_{water} is the friction factor of water under the same conditions. The purpose of PEC is to characterize the heat transfer performance of DPS under laminar flow conditions.

The PEC of Case 1 and Case 2 are shown in Fig.4.18 and Fig.4.19. It can be observed that that the flexible DPS lead to greater PEC values when compared to the more rigid DPS solutions. Furthermore, Fig. 4.19 indicates that greater inlet Reynolds number leads to slightly greater PEC values at the same axial distances and *m* values. All DPS lead to PEC values less than 1 because of the shear stress associated with DPS. In summary, rigidity of DPS should be controlled carefully to avoid low PEC values.

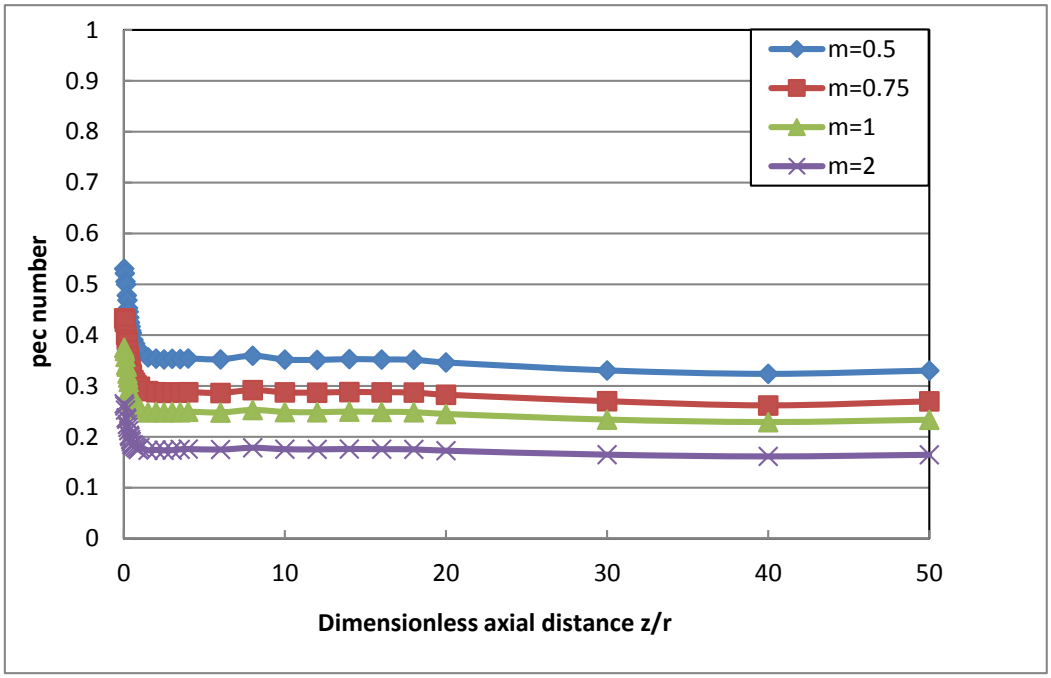

Fig. 4.18 Performance evaluation criteria of DPS in Case 1

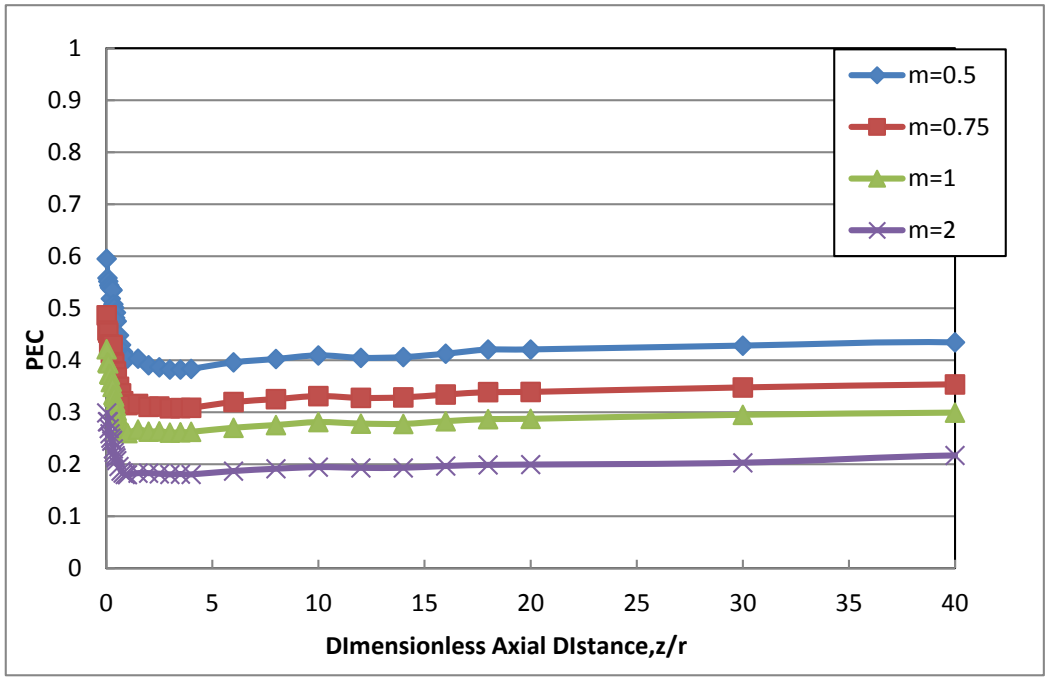

Fig. 4.19 Performance evaluation criteria DPS in Case 2

4.3 Comparison between Case 1 and Case 2

The Nusselt number for the same 0.2% xanthan solution with different inlet velocity are presented in Fig.4.20.

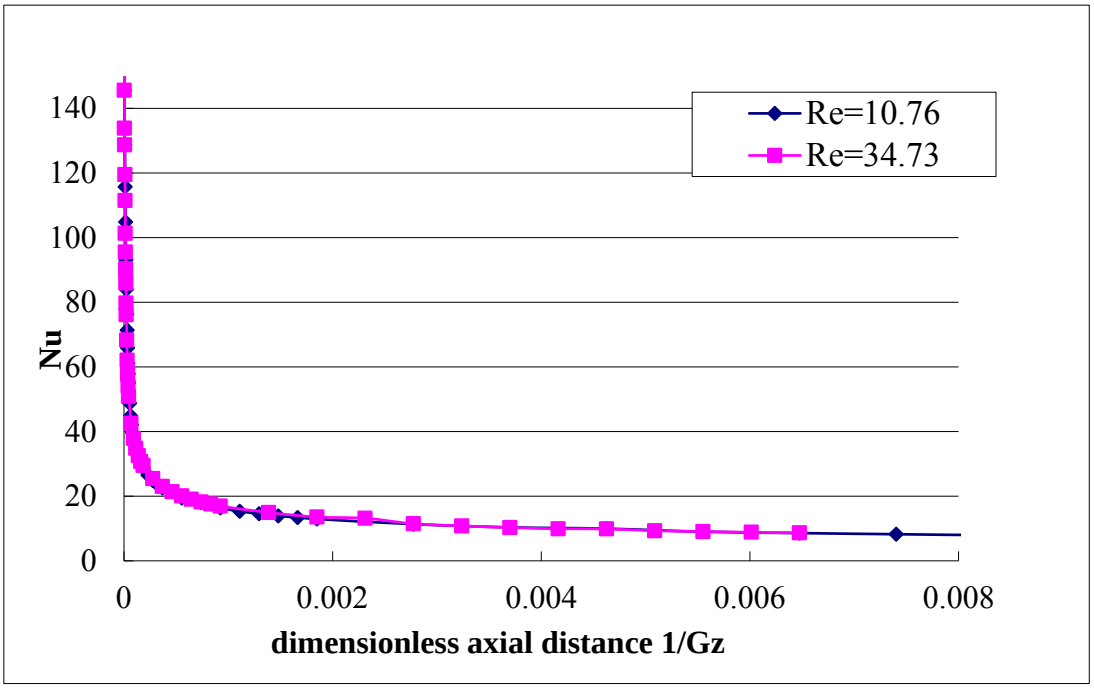

Fig. 4.20 Comparison of Nusselt number

It can be observed that the local Nusselt number of the same DPS with different Reynolds number do not vary much.

Friction factors of the same two DPS solutions with different Reynolds number are also shown in Fig.4.21. Thus the DPS with a higher Reynolds number leads to lower friction factor.

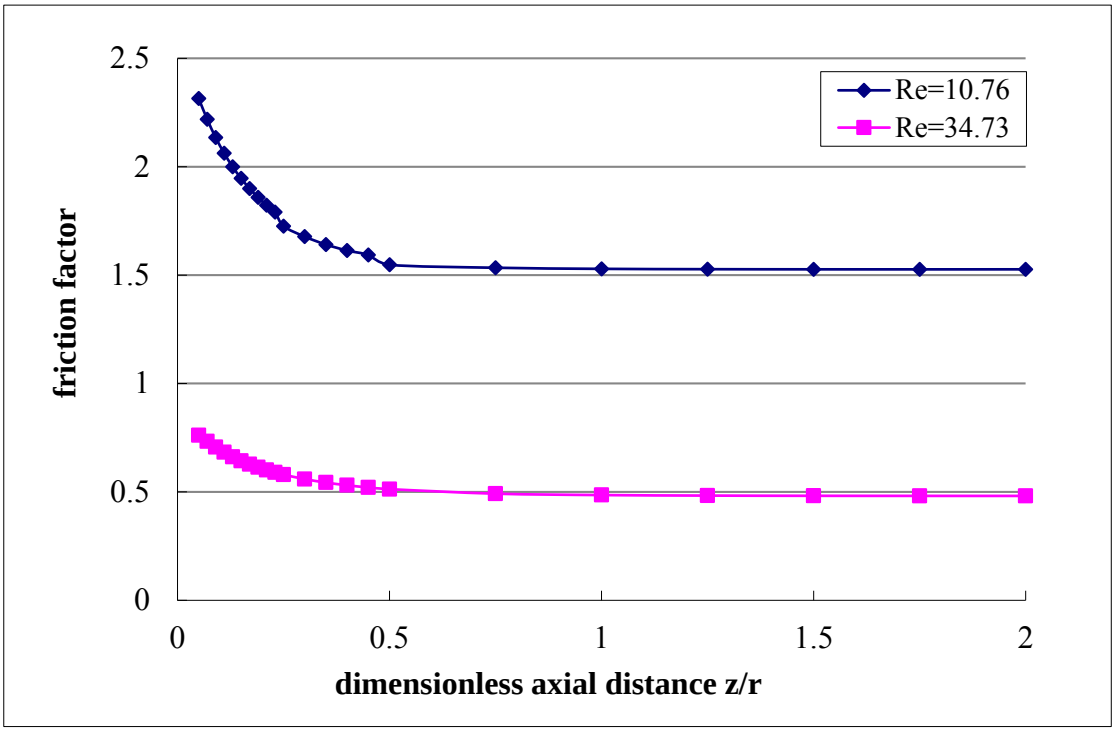

Fig. 4.21 Friction factor comparison of DPS with the same rigidity

PEC is also different between the two DPS because of different friction factor. It can be observed that a higher Reynolds number could lead to a higher value of PEC, which indicates that the heat transfer performance could be improved.

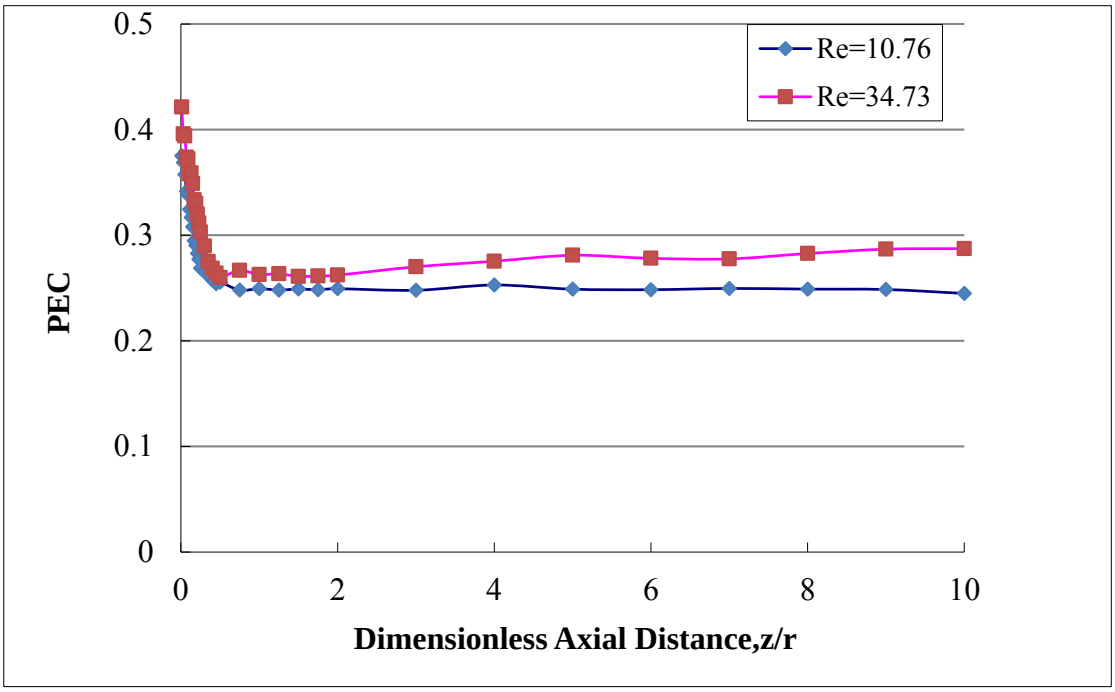

Fig. 4.22 PEC comparison of DPS with the same rigidity

The observations made during this study indicate that the polymer chain rigidity has a significant impact on the heat transfer performance of the dilute polymer solution in circular pipe with a constant wall heat flux. It can also be concluded that the Reynolds number also can influence the value of PEC and friction factor. Results indicate that polymer rigidity has little effect on how the local Nusselt number decreases with axial distance; however, DPS properties have a significant effect on the hydrodynamic behavior of DPS.

CONCLUSION

The effect of polymer rigidity on the heat transfer and rheological behaviors were investigated using a viscosity model for DPS with different rigidities. Constant wall heat flux and inlet plug velocity in a circular section were taken into consideration as boundary conditions. It was found that for the DPS, the polymer rigidity and the Reynolds number affect the friction factor behavior. A significant increase in the friction factor was observed when the rigidity changing parameter was set to higher values. Also, higher Reynolds number could lead to lower friction factor and slightly larger value of PEC. Furthermore, Reynolds number has little effect on Nusselt number even when using flexible polymers.

Experimental data are needed to validate the results presented in the current study. The current study also considered only laminar flow and 0.2% xanthan solution as DPS. Thus the effect of particles on the thermal performance has to be studied under laminar condition in a smooth circular tube taking into account the temperature dependence of viscosity and density to account for real conditions in heat exchangers.

REFERENCES

1. Ira M. Cohen, Pijush K. Kundu, Fluid Mechanics 4th edition, Academic Press, Burlington, MA, 2007.
2. A. H. P. Skelland, Non-Newtonian Flow and Heat Transfer, Wiley, New York, 1967.
3. Bingham, Eugene Cook, An investigation of the laws of plastic flow, Bulletin of the Bureau of Standards, 1916, Volume 13, Issue 2, 309.
4. Herschel, W.H., Bulkley, R, Konsistenzmessungen von Gummi-Benzollösungen, Kolloid Zeitschrift, 1926, Volume 39, 291–300.
5. Oswald-de Waele, Ueber die rechnerische Darstellung des Strukturgebietes der Viskosität, Colloid and Polymer Science, February 1929, Volume 47, Issue 2, 176-187.
6. Pierre J. Carreau, Ian F. MacDonald, R.Byron Bird, A nonlinear viscoelastic model for polymer solutions and melts, Chemical Engineering Science, August 1968, Volume 23, Issue 8, 901–911.

7. A. Mongruel, M. Cloitre, Axisymmetric orifice flow for measuring the elongational viscosity of semi-rigid polymer solutions, Journal Of Non-Newtonian Fluid Mechanics, 2003, Volume 110, Issue 1, 27-43.
8. M. V. Pastor, E. Costell, L. Izquierdo and L. Dunan, Effects of concentration, pH and salt content on flow characteristics of xanthan gum solutions, Food Hydrocolloids 1994, Volume 8, No.3-4, 265-275.
9. Vitaly O. Kheyfets,Sarah L. Kieweg, Gravity-driven thin film flow of an ellis fluid, Journal of Non-Newtonian Fluid Mechanics, December 2013, Volume 202, 88–98.
10. Graetz, L., Ueber die Wärmeleitungsfähigkeit von Flüssigkeiten, Annalen der Physik, 1885, Volume 261, Issue 7, 337–357.
11. Metzner, A. B., Vaughn, R. D. and Houghton, G. L. (1957), Heat transfer to non-newtonian fluids. AIChE Journal, 1957, Volume 3, Issue 1, 92-100.
12. R. Mahalingam, L. O. Tilton and J. M. Coulson, Heat Transfer in Laminar Flow of Non-Newtonian Fluids, Chemical Engineering Science. 1975, Volume 30. 921-929.
13. R.Mahalingam, S. F. Chan, J. M. Coulson, Laminar pseudoplastic flow heat transfer with prescribed wall heat flux, The Chemical Engineering Journal, 1975, Volume 9, Issue 2, 161–166.

14. D. A. Cruz, P. M. Coelho and M. A. Alves, A Simplified Method for Calculating Heat Transfer Coefficients and Friction Factors in Laminar Pipe Flow of Non-Newtonian Fluids, Journal of Heat Transfer, 2012, Volume 134, Issue 9, 091703.
15. R.P. Chhabra, J.F. Richardson, Non-Newtonian Flow and Applied Rheology Engineering Application, Amsterdam, Boston, MA, 2008.
16. M.P. Escudier, P.J. Oliveira, F.T. Pinho, S. Smith, Fully developed laminar flow of non-Newtonian liquids through annuli: comparison of numerical calculations with experiments, Experiments in Fluids, 2002, Volume 33, 101–111.
17. B.T.F. Chung & Z.J. Zhang, Heat transfer from thermally developing flow of non-Newtonian fluids in rectangular ducts, Transactions on Engineering Sciences, 1994, Volume 5.
18. E. SALEM and M. H. Embaby, Theoretical and experimental investigations of non-Newtonian fluid flow through non-circular pipes, Applied scientific research, 1977, Volume 33, Issue 2, 119 -139.
19. H. Pascal, F. Pascal, Flow of non-newtonian fluid through porous media, International Journal of Engineering Science, 1985, Volume 23, Issue 5, 571–585.

20. W. H. Suckow, P. Hrycak, R. G. Griskey, Heat Transfer to Polymer Solutions and Melts Flowing Between Parallel Plates, Polymer Engineering and Science, 1971, Volume 11, No. 5, 401-404.
21. Staudinger, H., Über Polymerisation. Berichte Der Deutschen, Chemischen Gesellschaft (A and B series), 1920, Volume 53, Issue 6, 1073–1085.
22. Alexander Yu. Grosberg, Alexei R. Khokhlov, Statistical Physics of Macromolecules, AIP Press, New York, 1994.
23. P. Debye, The Intrinsic Viscosity of Polymer Solutions, The Journal of Chemical Physics, 1946, Volume 14, 636.
24. Prince E. Rouse Jr., A Theory of the Linear Viscoelastic Properties of Dilute Solutions of Coiling Polymers, The Journal of Chemical Physics, 1953, Volume 21, 1272.
25. Bruno H. Zimm, Dynamics of Polymer Molecules in Dilute Solution: Viscoelasticity, Flow Birefringence and Dielectric Loss, The Journal of Chemical Physics, 1956, Volume 24, No. 2, 269.
26. O. Kratky, G. Porod (1949), Röntgenuntersuchung gelöster Fadenmoleküle Recueil des Travaux Chimiques des Pays-Bas, 1949, Volume 68, Issue 12, 1106–1122.
27. R.B. Bird, Charles F. Curtiss, Robert C. Armstrong, Ole H., Dynamics of Polymeric Liquids, Wiley, New York, 1987.

28. Michael D. Guiver, Young Moo Lee, Polymer Rigidity Improves Microporous Membranes, Science,18 January 2013, Volume 339, No. 6117, 284-285

29. J.M. Torres, C. Wang, E. Bryan Coughlin, John P. Bishop, Richard A. Register, Robert A. R., Christopher M. S., and Bryan D. V., Influence of Chain Stiffness on Thermal and Mechanical Properties of Polymer Thin Films, Macromolecules, 2011, Volume 44, Issue 22, 9040–9045.

30. Graham M. Harrison, Robert Mun, Graham Cooper, David V. Boger, Anote on the effect of polymer rigidity and concentration on spray atomisation, J. Non-Newtonian Fluid Mech. 1999, Volume 85, 93-104.

31. Jan-Michael Y. Carrillo and Andrey V. Dobrynin, Polyelectrolytes in Salt Solutions: Molecular Dynamics Simulations, Macromolecules 2011, Volume 44, 5798–5816.

32. I. Teraoka, Polymer Solutions: An Introduction to Physical Properties, Wiley, New York, 2002.

33. Kok, C. M. and Rudin, A. (1981), Relationship between the hydrodynamic radius and the radius of gyration of a polymer in solution, Die Makromolekulare Chemie, Rapid Communications, 16 November 1981, Volume 2, Issue 11, 655–659.

34. De Gennes, Brochard F., Collapse of one polymer coil in a mixture of solvents, Ferroelectrics, 1980, Volume 30, Issue 1, 33-47.

35. J. Higiro, T. J. Herald, S. Alavi, S. Bean, Rheological study of xanthan and locust bean gum interaction in dilute solution: Effect of salt, Food Research International, May 2007, Volume 40, Issue 4, 435-447.

36. Einstein, A., Über die von der molekularkinetischen Theorie der Wärme geforderte Bewegung von in ruhenden Flüssigkeiten suspendierten Teilchen, Annalen der Physik, 1905, Volume 322, Issue 8, 549–560.

37. Chong Meng Kok, Alfred Rudin, Relationship between the hydrodynamic radius and the radius of gyration of a polymer in solution, Makromol, Chem., Rapid Commun. 1981, Volume 2, 655 – 659.

APPENDIX A

USER DEFINED CODE.

Viscosity for Case: m=0.5

```
#include "udf.h"

DEFINE_PROPERTY(cell_viscosity, cell, thread)

{

    real visco;

    real mu;

    real R;

    R = C_STRAIN_RATE_MAG(cell,thread);

    mu = 0.64*0.353553*pow(R,-0.69)+0.000646447;

    if(mu > 0.001 && mu < 1000)

        visco = mu;

    else if(mu>=1000 )

        visco = 1000;

    else
```

```
        visco = 0.001;
    return visco;
    }
```

Viscosity for Case:m=0.75

```
#include "udf.h"
DEFINE_PROPERTY(cell_viscosity, cell, thread)
{
    real visco;
    real mu;
    real R;
    R = C_STRAIN_RATE_MAG(cell,thread);
    mu = 0.64*0.64952*pow(R,-0.69)+0.000350481;
    if(mu > 0.001 && mu < 1000)
        visco = mu;
    else if(mu>=1000 )
        visco = 1000;
    else
        visco = 0.001;
```

```
    return visco;
    }
    Viscosity for Case:m=1
#include "udf.h"
DEFINE_PROPERTY(cell_viscosity, cell, thread)
{
    real visco;
    real mu;
    real R;
    R = C_STRAIN_RATE_MAG(cell,thread);
    mu = 0.64*pow(R,-0.69);
    if(mu > 0.001 && mu < 1000)
        visco = mu;
    else if(mu>=1000 )
        visco = 1000;
    else
        visco = 0.001;
    return visco;
```

}

Viscosity for Case:m=2

```
#include "udf.h"
DEFINE_PROPERTY(cell_viscosity, cell, thread)
{
 real visco;
 real mu;
 real R;
 R = C_STRAIN_RATE_MAG(cell,thread);
 mu = 0.64*2.82843*pow(R,-0.69)-0.00182843;
 if(mu > 0.001 && mu < 1000)
      visco = mu;
 else if(mu>=1000 )
      visco = 1000;
 else
      visco = 0.001;
 return visco;
 }
```

APPENDIX B

Modeling Parameters for Smooth Circular Tube

a. Tube diameter: 0.02m

b. Dilute polymer solution concentration: 0.2%

c. Non-slip wall

d. Boundary Condition: Constant wall heat flux 100 W/m^2

e. Plug developed velocity at the inlet

	Density $kg\ m^{-3}$	Specific Heat $J\ kg^{-1}\ K^{-1}$	Thermal Conductivity $W\ m^{-1}\ K^{-1}$
Water	997	4180	0.606
Xanthan DPS	998	4128	0.6